



# A global marine particle size distribution dataset obtained with the Underwater Vision Profiler 5

Rainer Kiko<sup>1,\*</sup>, Marc Picheral<sup>1,\*</sup>, David Antoine<sup>2,1</sup>, Marcel Babin<sup>3</sup>, Léo Berline<sup>4</sup>, Tristan Biard<sup>5</sup>, Emmanuel Boss<sup>6</sup>, Peter Brandt<sup>7,8</sup>, Francois Carlotti<sup>4</sup>, Svenja Christiansen<sup>9</sup>, Laurent Coppola<sup>1</sup>, Leandro de la Cruz<sup>10</sup>, Emilie Diamond-Riquier<sup>1</sup>, Xavier Durrieu de Madron<sup>11</sup>, Amanda Elineau<sup>12</sup>, Gabriel Gorsky<sup>1</sup>, Lionel Guidi<sup>1</sup>, Helena Hauss<sup>7</sup>, Jean-Olivier Irisson<sup>1</sup>, Lee Karp-Boss<sup>6</sup>, Johannes Karstensen<sup>7</sup>, Dong-gyun Kim<sup>13</sup>, Rachel M. Lekanoff<sup>14</sup>, Fabien Lombard<sup>1</sup>, Rubens M. Lopes<sup>10</sup>, Claudie Marec<sup>3</sup>, Andrew M.P. McDonnell<sup>14</sup>, Daniela Niemeyer<sup>7</sup>, Margaux Noyon<sup>15</sup>, Stephanie H. O'Daly<sup>14</sup>, Mark Ohman<sup>16</sup>, Jessica L. Pretty<sup>14</sup>, Andreas Rogge<sup>17,13</sup>, Sarah Searson<sup>18</sup>, Masashi Shibata<sup>19</sup>, Yuji Tanaka<sup>20</sup>, Toste Tanhua<sup>7</sup>, Jan Taucher<sup>7</sup>, Emilia Trudnowska<sup>21</sup>, Jessica S. Turner<sup>22</sup>, Anya Waite<sup>23</sup>, and Lars Stemmann<sup>1</sup>

<sup>1</sup>Sorbonne Université, CNRS, UMR 7093, Laboratoire d'Océanographie de Villefranche-sur-Mer (LOV), Villefranche-sur-Mer, France

<sup>2</sup>Remote Sensing and Satellite Research Group, School of Earth and Planetary Sciences, Curtin University, Perth, WA 6845, Australia

<sup>3</sup>Département de Biologie, Université Laval, Québec, Canada

<sup>4</sup>MIO, Aix Marseille Univ., Université de Toulon, CNRS, IRD, MIO, Marseille, France UMR 7294 Mediterranean Institute of Oceanography, Marseille, France

<sup>5</sup>Univ. Littoral Côte d'Opale, Univ. Lille, CNRS, UMR 8187 - LOG - Laboratoire d'Océanologie et de Géosciences, F-62930 Wimereux, France

<sup>6</sup>School of Marine sciences, University of Maine, Orono, Massachusetts, USA

<sup>7</sup>GEOMAR Helmholtz Centre for Ocean Research Kiel, Kiel, Germany

<sup>8</sup>Faculty of Mathematics and Natural Sciences, Kiel University, Kiel, Germany

<sup>9</sup>Department of Biosciences, University of Oslo, Oslo, Norway

<sup>10</sup>University of São Paulo, Oceanographic Institute, São Paulo, Brazil

<sup>11</sup>CEFREM, CNRS-Université de Perpignan Via Domitia, Perpignan, France

<sup>12</sup>Institut de la Mer de Villefranche, CNRS - Sorbonne Université, Villefranche-sur-Mer, FRANCE

<sup>13</sup>Alfred-Wegener-Institut Helmholtz-Zentrum für Polar- und Meeresforschung, Bremerhaven, Germany

<sup>14</sup>College of Fisheries and Ocean Sciences, University of Alaska Fairbanks, Fairbanks, Alaska, USA

<sup>15</sup>Nelson Mandela University, Institute for Coastal and Marine Research, Gqeberha, South Africa

<sup>16</sup>Scripps Institution of Oceanography, La Jolla, California, USA

<sup>17</sup>Institute for Ecosystem Research, Kiel University, Kiel, Germany

<sup>18</sup>National Institute of Water and Atmosphere Research, New Zealand

<sup>19</sup>SeaBreath Co., Ltd., Tokyo, Japan

<sup>20</sup>Tokyo University of Marine Science and Technology, Tokyo, Japan

<sup>21</sup>Department of Marine Ecology, Institute of Oceanology Polish Academy of Sciences, Sopot, Poland

<sup>22</sup>Department of Marine Sciences, University of Connecticut Avery Point, Groton, Connecticut, USA

<sup>23</sup>Dalhousie University, Halifax, Nova Scotia, Canada

\*These authors contributed equally to this work.

**Correspondence:** Rainer Kiko (rainer.kiko@obs-vlfr.fr)



**Abstract.** Marine particles of different nature are found throughout the global Ocean. The term "marine particles" describes detritus aggregates, fecal pellets, but also bacterio-, phyto-, zooplankton and nekton. Here we present a global particle size distribution dataset obtained with several Underwater Vision Profiler 5 (UVP5) camera systems. Overall, within the 64  $\mu\text{m}$  to about 50 mm size range covered by the UVP5, detrital particles are the most abundant component of all marine particles in this size range and thus measurements of the particle size distribution with the UVP5 can yield important information on detrital particle dynamics. During deployment, which is possible down to 6000 m depth, the UVP5 images a volume of about 1 L at a frequency of 6 to 20 Hz. Each image is segmented in real time and size measurements of particles are automatically stored. All UVP5 units used to generate the here presented dataset were inter-calibrated using a UVP5 High Definition unit as reference. Our consistent particle size distribution dataset contains 8805 vertical profiles collected between 2008-06-19 and 2020-11-23. All major ocean basins, as well as the Mediterranean and the Baltic Sea were sampled. 19% of all profiles had a maximum sampling depth shallower than 200 dbar, 80% had a maximum sampling depth greater than 200 dbar, 38% sampled at least the upper 1000 dbar depth range and 11% went down to at least 3000 dbar depth. First analysis of the particle size distribution dataset shows that particle abundance is found to be high at high latitudes and in coastal areas where surface productivity or continental inputs are elevated. Lowest values are found in the deep ocean and in the oceanic gyres. Our dataset should be valuable for more in-depth studies that focus on the analysis of regional, temporal and global patterns of particle size distribution and flux as well as for the development and adjustment of regional and global biogeochemical models. The marine particle size distribution dataset (Kiko et al., 2021) is available at <https://doi.pangaea.de/10.1594/PANGAEA.924375>.

## 1 Introduction

### 1.1 Nature and origin of marine particles

Bacterio-, phyto- and zooplankton, nekton, aggregates, marine snow, fecal pellets, biomineralized shells, mineral dust, precipitates, suspended clay and nowadays also plastics are part of the general marine particle size spectrum (Sheldon and Parsons, 1967; Stemmann and Boss, 2012; Cózar et al., 2014). The relative contribution of living, detrital and abiotic particles to the total load of particles is not well known and may vary according to the particle size range and the marine ecosystem investigated from 1% to 50% (Forest et al., 2012; Stemmann and Boss, 2012; Checkley Jr et al., 2008). Abiotic particles can originate from resuspension at the seabed (Puig et al., 2013; McCave, 2009, 1986; Honjo et al., 1984), dust deposition (Zuniga et al., 2008; Ratmeyer et al., 1999) and influx by rivers (Ludwig and Probst, 1998) and glaciers (Neal et al., 2010). Furthermore, dissolved constituents precipitate when riverwater (Many et al., 2019) or hydrothermal fluids (German and Von Damm, 2003) mix with seawater. Photosynthesis by planktonic algae is the almost exclusive source of biogenic carbon in the open ocean, although other processes such as carbon fixation by chemoautotrophs (e.g., at hydrothermal vents), benthic algae, seagrass and, moreover, land and river derived organic particles add to this as well (e.g., Duarte et al. (2010); Ludwig and Probst (1998)). Higher trophic levels consume this biogenic carbon to build up biomass and fuel physiological activity. Along the entire plankton trophic web, part of the consumed carbon is also transformed into detritus (fecal pellets, exuviae, discarded houses or dead bodies). Small particles such as phytoplankton cells can also coagulate to form larger aggregates, that might also include other



35 detrital particles (Jackson, 1990). The two pathways lead to the formation of detrital particles, with different sinking properties  
depending on their size, content and porosity (Stemmann et al., 2004). As particle size is an essential trait for many biotic and  
abiotic interactions, it is often used to develop and calibrate size resolved mechanistic models of phytoplankton bloom forma-  
40 tion, particle coagulation and export to the mesopelagic zone (Stemmann et al., 2004; Jouandet et al., 2014; Bianchi et al.,  
2018). Moreover, the size structure of particles and plankton is one of the most relevant indicators of ecosystem functionality  
and energy fluxes (Jackson, 1990; Zhou; Stemmann and Boss, 2012). How abiotic and biotic marine particles of different sizes  
are formed, destroyed, advected or sink are key questions in ocean carbon cycling and biogeochemistry (Stemmann et al.,  
2012; Boyd et al.; Giering et al., 2020) and therefore their quantitative monitoring is needed.

### 1.2 Marine particle imaging

Many phyto- and zooplankton organisms, but also some other particles are sturdy and can be sampled using nets, traps, sedi-  
ment traps, bottles and in situ filtration devices. Fragile particles often formed by aggregation of diverse source particles (dead  
45 cells, fecal pellets, exudates, minerals) called "Marine snow" (Beebe, 1931) and fragile zooplankton such as cnidarians, rhizar-  
ians and other gelatinous organisms are however not amenable to such sampling methods (O'Hern et al.; Alldredge and Silver,  
1988; Wiebe and Benfield, 2003; Remsen et al., 2004). Therefore, only in situ measurements allow for a realistic assessment of  
the size and abundance of marine particles (Alldredge and Silver, 1988). Earliest such measurements were made from moored  
platforms, submersibles or by divers and included analyses of photographic images (Suzuki and Kato, 1953; Alldredge and  
50 Gotschalk, 1988). Advancement in electronic components and digital processing routines then allowed for the development  
of instruments such as the optical plankton counter (Herman, 1992), holographic instruments Katz et al. (1999) and various  
camera systems Asper (1987); Honjo et al. (1984); Lampitt et al. (1993); Ratmeyer and Wefer (1996); Benfield et al. (2007).  
Among them the Underwater Vision Profilers (UVP) Gorsky et al. (2000); Picheral et al. (2010) was designed to automatically  
size and count undisturbed abiotic and biotic marine particles.

55

### 1.3 The Underwater Vision Profiler and its use

The UVP was developed at the Laboratoire d'Océanographie de Villefranche (LOV) to provide consistent measurements of  
particle abundance and size. Single units of UVP versions 1 to 4 were produced from 1991 to 2008 (Gorsky et al., 2000,  
2002). The first prototype (sn000) of version 5 started field operations in 2008 and was described in detail by Picheral et al.  
60 (2010). The instrument was commercialised in 2010 and produced until 2021. A standard (STD) version with a 1.3 Megapixel  
greyscale camera was produced between 2008 and 2016 (serial numbers 000 to 011) and a high-definition (HD) version with  
a 4 Megapixel greyscale camera was produced between 2016 and 2021 (serial numbers 200 to 223). The smaller and more  
versatile UVP6 (Picheral et al., 2022) is commercially available since 2019. In the standard setting, the UVP5 images a volume  
of about 1 L at a frequency of 6 to 20 Hz and can be deployed down to 6000 m depth. Particles on each image are automatically  
65 sized. Further data processing of all particles allows calculations of the particle size distribution - the particle abundance or  
biovolume in increasing size intervals. The UVP5 STD version covers the size range from 102  $\mu\text{m}$  to  $\sim 50$  mm ESD, the HD



version the size range from 64  $\mu\text{m}$  to  $\sim 50$  mm ESD. Through reduction of the distance between the LED lights and the camera, the resolution can be further increased, but then the imaged volume is reduced. Inter-calibrated UVP5 units are globally in use by several teams. Since the UVP5 is mostly integrated in the CTD-Rosette and has its own pressure sensor, fine-scale vertical distribution of particles and major plankton groups can be related to environmental data obtained with other sensors mounted on the CTD-rosette. Most efforts regarding the analyses of UVP particle size spectra (including data from earlier versions such as the UVP4) have been on the estimation of particle biomass and flux by comparing them with particulate organic carbon (POC) collected in sediment traps or Niskin bottles (e.g., (Guidi et al., 2008b, 2015; Kiko et al., 2017; Stemmann et al., 2002, 2008a)). Particle abundance data was also used to estimate aerobic (Kalvelage et al., 2015; Thomsen et al., 2019) and anaerobic respiration (Bianchi et al., 2018; Karthäuser et al., 2021), to inform model development (Bianchi et al., 2018; Stemmann et al., 2004; Jouandet et al., 2014) or calibrate biogeochemical models (Niemeyer, 2020). Changes in the particle distribution were related to physical processes such as transport along continental margins (Stemmann et al., 2008b; Forest et al., 2013; de Madron et al., 1999), deep resuspension (Puig et al., 2013; de Madron et al., 2017) and mesoscale processes (Waite et al., 2016; Fiedler et al., 2016; Stemmann et al., 2008b; Guidi et al., 2012). Profound changes in bacterial activity at Oxygen minimum zone boundaries (Roullier et al., 2014) were related to enhanced particle abundance. Likewise, the importance of phyto- (Stemmann et al., 2002; Guidi et al., 2009) and zooplankton (Hauss et al., 2016; Christiansen et al., 2018; Stemmann et al., 2004) interactions with particles were assessed and the introduction of particles at depth via zooplankton Diel Vertical Migration reported (Kiko et al., 2017, 2020; Stemmann et al., 2000). In recent years, image analysis of large objects was performed and plankton organisms were discriminated from the detrital and abiotic particles in subsets of the dataset presented here, allowing the study of large plankton communities (Forest et al., 2012), bio-geography of specific taxa (Christiansen et al., 2018; Biard et al., 2016), zooplankton functional traits (Vilgrain et al., 2021) and particle types (Trudnowska et al., 2021).

#### 1.4 The global marine particle size distribution dataset

Here we provide a dataset that was obtained with several inter-calibrated UVP5 units operated by different laboratories and during different cruises and projects around the world (Table 1). This international, collaborative effort resulted in a consistent, inter-calibrated global marine particle size distribution database that contains 8805 particle abundance and biovolume profiles obtained in all major oceans and several marginal seas since 2008. We provide further details about the UVP5, the inter-calibration and quality control procedures and the dataset structure in the Material and Methods section. Summarizing statistics, maps on data distribution, a description of global particle distribution and recommendations for use and further growth of the dataset are provided in the Results and Discussion sections.



## 95 2 Material and Methods

### 2.1 UVP5 description

The UVP5 consists of one downward-facing camera in a titanium pressure case and two sets of red LED lights that illuminate a 0.88 to 1.16 L-water volume Picheral et al. (2010). The imaged volume depends on the actual instrument set-up which was determined experimentally for each set-up. During deployment - usually during the downcast of a CTD profile - the UVP5 takes  
100 5-20 pictures of the illuminated volume of water per second. The particles in each image are counted and sized immediately and the data are stored in the instrument. Particle area is measured as the number of pixels ( $Sp$ ) of an imaged object and can be converted to particle cross-sectional area ( $Sm$ ) in  $mm^2$  using:  $Sm = Aa * Sp^{Exp}$ . Here,  $Aa$  represents the area of one pixel in  $mm^2$ .  $Exp$  is a dimensionless adjustment factor.  $Aa$  and  $Exp$  need to be calibrated experimentally. To conduct the initial calibration for the dataset provided here, natural plankton and particle objects from the Bay of Villefranche-sur-Mer, France,  
105 were imaged in an aquarium with the UVP5 HD sn203 and using a stereo microscope during experiments conducted in fall 2016. Optimal values for the parameters  $Aa$  and  $Exp$  were obtained by minimizing  $\Delta S$ , defined as

$$\Delta S = \sum_i (\log(Aa \cdot S_{i,p_u}^{Exp}) - \log(S_{i,m_\mu}))^2$$

where  $S_{i,p_u}$  is the surface area in pixels of object  $i$  as seen by the UVP and  $S_{i,m_\mu}$  is the surface area in  $mm^2$  of the same object  $i$  measured under the stereomicroscope. The minimization was performed using the Nelder-Mead simplex algorithm (implemented in the MATLAB function *fminsearch*). For this calibration experiment an  $Aa$  of  $0.0036 mm^2$  (interquartile  
110 range from  $-0.0002$  to  $0.0074 mm^2$ ), an  $Exp$  of  $1.149$  (interquartile range  $1.016$  to  $1.282$ ) and an  $r^2$  of  $0.88$  were found. Further details regarding the initial calibration procedure for the UVP5 SD version that was also applied to obtain the UVP5 HD calibration coefficients are given in Picheral et al. (2010).

### 2.2 Instrument inter-calibration

As several UVP5 units were produced, an inter-calibration procedure was developed to allow comparability of data from these  
115 units. The inter-calibration procedure is based on a comparison between one or several reference units (in particular sn002 and sn203) and the units to be calibrated. The imaged volume of each unit is determined, before the instruments are deployed at sea simultaneously on the same instrument carrier and the normalized size spectra are calculated. These operations have been performed since 2008 in the Mediterranean Sea off Nice, France. Figure 1a shows an example of raw data from a parallel deployment of a reference unit (sn002) and a unit under calibration (sn200). The  $Aa$  and  $Exp$  of the sn200 is then adjusted,  
120 so that after post-processing the normalized size spectra of both units coincide (Figure 1b). The reference units were regularly inter-calibrated against each other to check for possible drifts and improved data consistency. The development of the HD version of the UVP5 in 2016 required a revision of the UVP5 inter-calibration procedure, as pixel resolution has changed (Picheral et al., 2010). The calibration obtained for the HD unit sn203 in fall 2016 was propagated to several STD model reference units via simultaneous deployment at sea and subsequent calculation of correction factors. Thereafter, the corrections



125 obtained for the reference units were digitally propagated to all previously used UVP5 by reanalysing the earlier calibration  
experiment data. How the uncertainties of the initial calibration of the HD model sn203 propagate to the other UVP5 units and  
if these uncertainties can be reduced need to be further investigated.

### 2.3 Data collection, processing, quality control and dataset description

Metadata (position, time) of each profile collected in the presented dataset were checked by the respective data owners.  
130 All instrument settings and calibration coefficients for all cruises and projects were checked and, if necessary, corrected to  
match the HD inter-calibration results using automatic routines. Data from all cruises were then reprocessed using Zoopro-  
cess (<https://sites.google.com/view/piqv/zooprocess>) to obtain a coherent and inter-calibrated dataset, based on the HD inter-  
calibration conducted in fall 2016. For easier access and preliminary sharing, the data were then uploaded to EcoPart ([http://ecopart.obs-  
vlf.fr](http://ecopart.obs-<br/>vlf.fr)). To enable the archiving at Pangaea, data were directly downloaded from the EcoPart SQL database using a dedicated  
135 Python script and separated into three-year splits to obtain smaller file sizes and to enable the subsequent addition of further  
data.

During processing, the silhouette area of each particle is calculated as described above and then converted to an equivalent  
spherical diameter (ESD) according to  $ESD = \sqrt{4 * Sm / \pi}$ . Biovolume is calculated assuming a spherical particle using  
140  $Biovolume = ESD^3 * \pi / 6$ . Particles in a certain size class (e.g., ESD: 0.0403 - 0.0508 mm) and within a 5 dbar depth range  
are then counted and divided by the total observed volume to yield the particle abundance (#/L) in this size and depth interval.  
Likewise, the biovolume of individual particles is added up and divided by the observed volume to yield biovolume in  $mm^3/L$ .  
Size class bins are evenly spaced in a natural logarithmic scale, starting at 0.001 mm and ending at 26 mm, with in total 45 size  
bins. Size class bin width is hence increasing with size in a logarithmic fashion. Due to the detection limits of the UVP5, size  
145 class bins smaller 0.0403 mm ESD are empty and not reported, the largest size bin covers the size range from 20.6 to 26 mm  
ESD. Particle abundance and biovolume of particles with an ESD > 26 mm is also provided as an additional value. Data in this  
form is available on the EcoPart server. Quality-checked data was downloaded from the server on May 26, 2021 and submitted  
to Pangaea (<https://doi.pangaea.de/10.1594/PANGAEA.924375>). Apart from the particle abundance and biovolume in different  
size classes, the dataset contains the cruise id, the EcoPart Project identifier (integer), the Profile identifier, the filename of the  
150 raw file, the filename of an accompanying ctd profile (if this exists), latitude, longitude (both in decimals), date and time (in  
UTC), an EcoPart internal station identifier (integer), depth (indicated via the middle value of the 5 dbar depth bin; in dbar) and  
the observed volume per depth bin (in L). The particle size distribution data reported is inclusive of all living and non-living  
particles across the size range of detection. The dataset (available at <https://doi.pangaea.de/10.1594/PANGAEA.9243751>) con-  
tains all individual profile data. Also the values of *AA*, *Exp* and the imaged volume for each data acquisition are archived at  
155 Pangaea in the "Metadata collection for a global marine particle size distribution dataset obtained with the Underwater Vision  
Profiler 5" (available at: [https://download.pangaea.de/reference/106293/attachments/Project\\_metainfo\\_for\\_Pangaea-4.txt](https://download.pangaea.de/reference/106293/attachments/Project_metainfo_for_Pangaea-4.txt)), to-  
gether with the dataset presented here. To enable visualization within this article, we aggregated particle abundance as in Kiko  
et al. (2017) into micrometric- (MiP: 0.14 to 0.53 mm ESD) and macroscopic particles (MaP: 0.53 mm to 16.88 mm ESD), and



calculated the slope  $k$  of the differential particle size distribution as a descriptor of the relationship between particle abundance  
and size (Stemmann and Boss, 2012). This relationship is generally approximated by a two-parameter power-law function:  
 $N = bd^{-k}$ , where  $b$  and  $k$  are constants and  $d$  is the mean particle diameter for a given diameter range ( $dr$ ). The differential  
particle abundance  $N$  can be calculated as the total number of objects per unit volume in the given diameter range  $dr$  (e.g.  
0.203 mm to 0.256 mm) divided by the diameter range (in this case 0.053 mm) and is given as the number of particles per  
volume per size. To obtain an estimate of  $k$ , which is also referred to as the slope of the particle size distribution, one can then  
conduct a linear regression of  $\log(N)$  vs.  $\log(d)$  as  $\log(N) = \log(b) - k(\log(d))$ . The PSD slope  $k$  is calculated for the size  
range 0.203 mm to 2.05 mm, as this is the size range where the slope is mostly linear. These slope  $k$  is only considered if the  
p-value of the regression is  $< 0.05$ , otherwise the value is set to *nan* (not a number).

Already published datasets (Table 2) use different calibration coefficients which are not consistent with the HD inter-  
calibration procedure and differences may arise when comparing the different versions. As an example we calculated abun-  
dances of two size classes and spectral slopes using the datasets from RV Maria S Merian cruise MSM23 and several RV  
Meteor cruises. MiP abundances are 4.2 (median; interquartile range 3.8 to 4.7) times larger with the new calibration factors,  
whereas MaP abundances are 1.5 times larger (median; interquartile range 1.2 to 2.0). Estimates of the slope  $k$  of the PSD are  
1.09 (median; interquartile range 1.05 to 1.12) times larger. These factors were calculated using the datasets from RV Maria S  
Merian cruise MSM23 and RV Meteor cruises M92, M96 and M107 for which archived datasets with the relevant data exist.

We do not distinguish UVP5 particle data into distinct categories, such as copepods, aggregates, fecal pellets or other  
taxonomic or morphologic classes. For UVP5 data, this is possible for objects  $> 1$  mm ESD, as the UVP5 also retrieves  
"vignettes" - small thumbnail images of respective regions of interest. Homogeneous identification of these vignettes among  
different cruises and operators is a time-consuming task and was not yet achieved for the entire dataset. Data from a subset of  
profiles are currently being prepared for publication.

## 3 Results and Discussion

### 3.1 Data distribution

The global distribution of UVP5 profiles contained in the published dataset is shown in Figure 2; in total, it comprises 8805  
profiles, collected between 2008-06-19 and 2020-11-23 and between 81.3695 °N and 75.289 °S. The dataset represents a  
compilation of particle data from numerous small regional-scale research cruises as well as several large-scale hydrographic  
transects with bathypelagic and cross-basin coverage. All major ocean basins, the Mediterranean and the Baltic Sea were  
sampled. Most data is available from the Mediterranean Sea, the tropical Atlantic and Pacific, the Gulf of Alaska and the  
Arctic. Information on the number of profiles obtained per year, month and depth level is shown in Figure 3. The majority of  
profiles was collected in the upper 1000 m of the water column in June and August. Between 217 and 1146 profiles per year  
were obtained between 2008-2018. Almost all UVP5 data obtained between 2008 and 2019 are contained in our dataset. We  
were not able to obtain data from all UVP5 owners and can therefore not provide an exact estimate of how many profiles are  
currently missing from the dataset. Furthermore, some datasets obtained in 2019 and 2020 still require processing and will be



added in subsequent updates of the dataset. Sampling effort is biased to the Northern hemisphere summer. Of all 8805 profiles, 1676 (19%) are shallower than 200 dbar, 7127 (80%) cover the upper 200 dbar of the water column, 3426 (38%) the upper 1000 dbar and 1018 (11%) go down to at least 3000 dbar. Deep profiles are mostly full depth profiles. The deepest profile reached 6017.5 dbar depth. Figure 4 shows the maximum depth per 2 degree grid box, whereas figure 5 shows the number of profiles obtained per 2 degree grid box.

### 3.2 Global particle abundance patterns

The global UVP5 particle dataset enables the characterisation of particle abundance and size structure patterns at a global scale, but also enables specific insights into particle dynamics at several regional study sites (e.g., the Gulf of Alaska, the California, Humboldt, Benguela and Mauretania upwelling systems and the Mediterranean Sea). Here, we aim to provide a short description of global particle distribution patterns and reference a few, already published studies. We use the terms micrometric particles (MiP) for particles with 0.14 to 0.53 mm ESD and macroscopic particles (MaP) for particles with 0.53 mm to 16.88 mm diameter) as in Kiko et al. (2017). Thereby, we also follow an approach used for marine aggregates, where those larger than 0.5 mm ESD are defined as marine snow (Suzuki and Kato, 1953; Alldredge and Silver, 1988). Globally, MiP and MaP concentrations in the upper 200 m are very variable (Figures 6, 9). High MiP and MaP particle abundance in coastal regions, in upwelling or frontal zones (MiP maximum values > 50000 #/L, MaP maximum values > 2000 #/L) are likely due to higher biological production and coastal inputs (Guidi et al., 2008a; Stemmann et al., 2008b; Roullier et al., 2014; Kiko et al., 2017). Particle concentrations are lower in oligotrophic gyres (MiP minimum values: 0.81 #/L MaP minimum values, 0.0 #/L MaP) where productivity and advective input from coastal regions are low (Guidi et al., 2008a, 2009; Stemmann et al., 2008a; Guidi et al., 2015). Particle abundance generally declines from the surface to depth (compare Figures 5, 6 and 7, as well as 8, 9 and 10). MiP and MaP in the meso- and bathy-pelagic layers also show a pattern consistent with the upper surface pattern probably as a consequence of passive flux of sinking particles (Guidi et al., 2015) and the active supply of particles via diel vertical migrations of zooplankton and nekton to the mesopelagic (Kiko et al., 2017, 2020). The strength of these supply mechanisms is dependent on the biological productivity at the surface, the strength of the active transport processes and the attenuation processes in the mesopelagic (Guidi et al., 2009). For the following analyses of vertical particle distribution in the open ocean, we only use data from profiles that were conducted down to at least 3000 dbar. For this subset, we find that MiP concentrations range from 0.81 to 53486.0 #/L between 0-200 dbar (mean: 315.67, std: 1269.53), 1.29 to 38580.0 #/L between 200-1000 dbar (mean: 54.39, std: 228.86) and 0.7 to 3184.0 #/L between 1000-3000 dbar (mean: 15.47, std: 23.76). MaP concentrations ranging from 0.0 to 2130.1 #/L between 0-200 dbar (mean: 6.17, std: 47.52), 0.0 to 2560.0 #/L between 200-1000 dbar (mean: 0.89, std: 5.17) and 0.0 to 77.77 #/L between 1000-3000 dbar (mean: 0.16, std: 0.57). The decline of particle abundance with depth has been interpreted as a consequence of microbial and metazoan flux attenuation (Stemmann et al., 2004; Guidi et al., 2009). The variability in MiP and MaP abundance range also decreases from the epi- to the bathy-pelagic, suggesting a feedback mechanism where high particle abundance results in strong flux attenuation by metazoans, thereby removing peaks in particle abundance and flux (Guidi et al., 2009).





### 225 3.3 Slope of the particle size distribution

The size distribution of particles is a basic property of marine systems, affecting trophic interactions, the vertical transmission of solar energy and the downward transport of organic matter Stemmann and Boss (2012). Despite its fundamental importance, size distribution is difficult to measure because particles occur over a large range of size and composition, from sub-micrometer compact particles to large, cm-sized loose aggregates (Jackson et al., 1995; Stemmann et al., 2008a; Lombard et al., 2019).  
230 We here use the differential particle size distribution as e.g. described by Stemmann and Boss (2012). A slope  $k$  of 4 of the differential particle size distribution suggests an equal amount of mass in logarithmic increasing size intervals. By combining instruments over a  $\mu\text{m}$  to cm size range it was shown that the value of the slope varies greatly around the typical value of 4 Jackson et al. (1995); Stemmann et al. (2008a). Our study also shows that the slope  $k$  varies greatly in the epi-, meso- and bathypelagic (Figures 12, 13 and 14). If we constrain the dataset to profiles that go deeper than 3000 dbar, the global mean  
235 value of the slope  $k$  in the top 200 dbar of the water column is found to be  $-3.57 \pm 0.56$  std (minimum  $-6.58$ , maximum  $-1.8$ ), with significant variations from  $-4$  which are likely due to local ecosystem processes and other impacts. The average slope  $k$  and the variability remain similar at greater depth ( $-3.59 \pm 0.67$  std, minimum  $-8.25$ , maximum  $-1.37$  at 200-1000 dbar depth,  $-3.52 \pm 0.6$  std, minimum  $-7.34$ , maximum  $-1.33$  at 1000 to 3000 dbar depth). Throughout all depth ranges, steepest slopes are observed in oligotrophic basins such as the Eastern Mediterranean Sea and the center of the South Pacific gyre, while  
240 flatter spectra are observed in more productive regions such as the Western Mediterranean Sea and at high latitudes. These observations confirm earlier work using more restricted datasets (Guidi et al., 2009; Stemmann et al., 2008c; Guidi et al., 2008a). Earlier work based on a sub-sample of the dataset has also shown that the slope of the size spectrum is correlated with the phytoplankton community composition (Guidi et al., 2009; Stemmann et al., 2002) and can show diel variability related to zooplankton migration (Stemmann et al., 2000). Deeper in the water column, the spatial pattern of the slope  $k$  mostly reflects  
245 the upper ocean variability. Interestingly, bathypelagic values of  $k$  in the Antarctic are relatively flat, compared to temperate and tropical regions, which suggests that, in the Antarctic deep sea the relative role of larger, aggregated particles is more important than in the temperate and tropical regions. Such trend is not observed in data from Arctic regions.

### 3.4 Potential uses of the data

A further, detailed analysis of the provided dataset is beyond the scope of this article. Observation of a particle at a certain depth  
250 always generates the question how it was formed or arrived at the given location. Many attempts have been carried out to relate the UVP particle size spectrum with flux measured in sediment traps or by Thorium (Guidi et al., 2008b; Forest et al., 2013; Guidi et al., 2015), sinking speed (Stemmann et al., 2002) and POC (Stemmann et al., 2008a) but deriving biogeochemical properties from particle size is certainly an area for future progress. In these regards, our dataset should enable further regional and global analyses of particle dynamics (see e.g. Bisson et al. (2021)) and - in combination with flux estimates from sediment  
255 traps and/or Thorium isotope measurements, but also environmental data from satellites and other sources - enable us to better constrain the particle flux component of the biological pump (see e.g., Clements et al. (2021b, a)). However, we would like to stress that although the particles in our dataset are not per se sinking (e.g., also living zooplankton are treated as particles),



particle abundance and size alone are still important information. Therefore, the data is also especially useful to constrain models that explicitly generate a particle size spectrum (Bianchi et al., 2018; Niemeyer, 2020; Weber and Bianchi, 2020; 260 Stemann et al., 2004; Jouandet et al., 2014). On the other hand particle data can also be used to estimate remineralization rates (Kalvelage et al., 2015; Bianchi et al., 2018; Thomsen et al., 2019; Karthäuser et al., 2021) or study trace element scavenging.

### 3.5 Recommendations for further instrument usage and growth of the dataset

This work presents the first attempt to establish a calibrated global data set of UVP measurements. Our analysis led us to 265 develop a set of recommendations for future expansion of the global UVP data set. First of all, we recommend that full depth profiles are always taken at locations shallower than 1000 m depth and that otherwise at least the full mesopelagic down to 1000 m depth be sampled when using the UVP5. This is motivated by the fact that particle processes (indicated via a large range of e.g., MiP and MaP abundance) at these depths are very dynamic and require high resolution sampling. Below 1000 m depth, particle spatial patterns are less variable. Nevertheless, if sampling during a research cruise is conducted at water depths 270 > 1000 m, full depth profiles or profiles down to the maximum depth rating of the used instruments (typically 6000m) should be done as often as possible. The deep sea is not well characterized with respect to abundance and size of particles and these comparatively small demands on shiptime will generate an important added value, as this will e.g. enable us to further assess carbon sequestration in the deep sea. Regions that are not well sampled until now are the Indian Ocean, Antarctic waters and the Western Pacific. Furthermore, winter data from both hemispheres is mostly lacking as well. In general, the UVP should be 275 used during repeat hydrography programs as the operational goals of these programs to cover a representative fraction of the ocean (global and full depth coverage) align with our goals to create a global particle size distribution dataset. SCOR working group 154 "Integration of Plankton-Observing Sensor Systems to Existing Global Sampling Programs (P-OBS)" recommended the use of the UVP during the GO-ship program and similar sea-going expeditions (Boss et al., 2020). Data from the smaller and more versatile UVP6 (Picheral et al., 2022) that can also be deployed on gliders, floats, moorings and other vectors should 280 also be integrated in future datasets and will enable the study of particle dynamics at spatial and temporal scales that are not accessible with the UVP5. Ancillary data that is useful for the interpretation of UVP data are temperature, salinity, oxygen and nutrient measurements, measurements of current dynamics, but also any measurements of particle dynamics and characteristics (e.g., Thorium-isotope measurements, lipid-content, elemental composition, particle sinking speed, sedimentation flux) and data on bacterio- phyto- and zooplankton composition. The latter are especially needed to understand the ecological processes 285 behind the observed size spectra of particles and their subsequent export. The evaluation of the relative proportions of living and non-living particles is particularly important at the large size range (few hundreds of micrometer) because large, possibly sinking particles may be confused with zooplankton and lead to overestimation of particle stock and flux (Kiko et al., 2020). In the future, better automatic image classification algorithms may help to discriminate between non-living particles and plankton organisms and even provide information on other properties than their size (Stemann and Boss, 2012; Trudnowska et al., 290 2021). We strongly recommend that regular inter-calibration experiments of all instruments against one or several standard units take place to maintain the data quality of all UVP units at an inter-operable level.



#### 4 Conclusions

Here we provide the first global particle size spectra dataset containing 8805 profiles that were obtained with the UVP5 between 2008 and 2020. All UVP5s used were inter-calibrated with a standard procedure, calibration coefficients and metadata were checked and all profile data were reprocessed. This dataset therefore is internally consistent and supersedes earlier versions of cruise-specific UVP5 particle size spectrum data. The analysis of this global dataset shows that particle abundances are high in regions of high primary productivity and in coastal areas. Further analysis of the dataset should enable insights on different aspects of particle dynamics such as the effects of mesoscale features and Oxygen Minimum Zones, the fate of particulate matter in the deep sea and many other important aspects of the oceans biogeochemistry.

#### 300 5 Data availability

The global UVP5 particle dataset Kiko et al. (2021) is publicly available at <https://doi.pangaea.de/10.1594/PANGAEA.924375>. The dataset was downloaded from the <https://ecopart.obs-vlfr.fr/> server on the 15. February 2022.

#### *Author contributions.*

RK, MP and LS formulated the goals for data aggregation, quality control and the publication of a global UVP5 dataset. RK and MP led the quality control endeavors, supported by all co-authors. RK and LS conceived and drafted the article. All authors participated writing the article.

#### *Competing interests.*

The authors declare no competing interest.

*Acknowledgements.* RK acknowledges support via a “Make Our Planet Great Again” grant of the French National Research Agency within the “Programme d’Investissements d’Avenir”; reference “ANR-19-MPGA-0012” and via EU H2020 grant (agreement 817578 TRIATLAS project). RK and HH furthermore acknowledge support by the DFG-funded collaborative research center 754 “Climate-biogeochemistry interactions in the tropical Ocean” (Work Package B8) and the “CUSCO—Coastal Upwelling System in a Changing Ocean” project (Grant no. 03F0813A; Work package 5) funded by the Federal Ministry of Education and Research (Germany). The McDonnell Laboratory at the University of Alaska Fairbanks acknowledges support from the U.S. National Science Foundation (Award numbers 1654663 and 1656070), the U.S. National Aeronautics and Space Administration (Award number 80NSSC17K0692), and the M.J. Murdock Charitable Trust. The collection of data by the University of Maine were funded by NASA grants NNX15AE67G (NAAMES) and 80NSSC17K0568 (EXPORTS). We thank the support of CNRS-INSU through the MISTRALS-MERMEX program. LS was supported by the Chair Vision between CNRS and Sorbonne University.



## References

- 320 Alldredge, A. L. and Gotschalk, C.: In situ settling behavior of marine snow I, *Limnology and Oceanography*, 33, 339–351, 1988.
- Allredge, A. L. and Silver, M. W.: Characteristics, dynamics and significance of marine snow, *Progress in oceanography*, 20, 41–82, 1988.
- Asper, V. L.: Measuring the flux and sinking speed of marine snow aggregates, *Deep Sea Research Part A. Oceanographic Research Papers*, 34, 1–17, 1987.
- Beebe, W.: A Round Trip to Davy Jones’s Locker, *National Geographic Magazine*, LIX, 1931.
- 325 Benfield, M. C., Grosjean, P., Culverhouse, P. F., Irigoien, X., Sieracki, M. E., Lopez-Urrutia, A., Dam, H. G., Hu, Q., Davis, C. S., Hansen, A., et al.: RAPID: research on automated plankton identification, *Oceanography*, 20, 172–187, 2007.
- Bianchi, D., Weber, T. S., Kiko, R., and Deutsch, C.: Global Niche of Marine Anaerobic Metabolisms Expanded by Particle Microenvironments, *Nature Geoscience*, 11, 263–268, <https://doi.org/10.1038/s41561-018-0081-0>, 2018.
- Biard, T., Stemann, L., Picheral, M., Mayot, N., Vandromme, P., Hauss, H., Gorsky, G., Guidi, L., Kiko, R., and Not, F.: In situ imaging  
330 reveals the biomass of giant protists in the global ocean, *Nature*, 532, 504–507, 2016.
- Bisson, K. M., Kiko, R., Siegel, D. A., Guidi, L., Picheral, M., Boss, E., and Cael, B. B.: Sampling uncertainties of particle size distributions and derived fluxes, <https://doi.org/10.1002/essoar.10508460.1>, <https://doi.org/10.1002/essoar.10508460.1>, 2021.
- Boss, E., Waite, A. M., Uitz, J., Acinas, S. G., Sosik, H. M., Fennel, K., Berman-Frank, I., Cornejo, M., Thomalla, S., Yamazaki, H., Batten, S., Berg, J., Claustre, H., Grégori, G., Karstensen, J., Muller-Karger, F., Richardson, A., Sloyan, B., Wanninkhof, R., Ras, J., Dimier, C.,  
335 Cetinić, I., Duforêt, L., Clemenston, L., Ferrera, I., Gasol, J. M., Massana, R., Sánchez, P., Sebastián, M., Sunagawa, S., Garczarek, L., de Vargas, C., Pesant, S., Mathew, S., Campbell, L., Brosnahan, M., Poulton, N., Marie, D., Gaube, P., Downie, R., Kloser, R., Lee, W.-J., Sato, M., Roesler, C., Dall’Olmo, G., Slade, W., Twardowski, M., Gardner, W., Briggs, N., Xing, X., Organelli, E., Frouin, R., Barone, B., McDonnell, A., Liu, Y., Chase, A., Miloslavich, P., Lombard, F., Behrenfeld, M., Jumars, P., and Karp-Boss, L.: Recommendations for plankton measurements on the GO-SHIP program with relevance to other sea-going expeditions, SCOR Working Group 154 GO-SHIP  
340 Report, 2020.
- Boyd, P. W., Claustre, H., Levy, M., Siegel, D. A., and Weber, T.: Multi-Faceted Particle Pumps Drive Carbon Sequestration in the Ocean, 568, 327–335, <https://doi.org/10.1038/s41586-019-1098-2>, <https://www.nature.com/articles/s41586-019-1098-2>.
- Checkley Jr, D., Davis, R., Herman, A., Jackson, G., Beanlands, B., and Regier, L.: Assessing plankton and other particles in situ with the SOLOPC, *Limnology and Oceanography*, 53, 2123–2136, 2008.
- 345 Christiansen, S., Hoving, H.-J., Schütte, F., Hauss, H., Karstensen, J., Körtzinger, A., Schröder, S.-M., Stemann, L., Christiansen, B., Picheral, M., et al.: Particulate matter flux interception in oceanic mesoscale eddies by the polychaete *Poecobius* sp., *Limnology and Oceanography*, 63, 2093–2109, 2018.
- Clements, D. J., Yang, S., Weber, T., McDonnell, A., Kiko, R., Stemann, L., and Bianchi, D.: Constraining the Ocean’s Biological Pump with in Situ Optical Observations and Supervised Learning. Part 2: Carbon Flux | Earth and Space Science Open Archive, <https://www.essoar.org/doi/10.1002/essoar.10509084.3>, 2021a.  
350
- Clements, D. J., Yang, S., Weber, T., McDonnell, A., Kiko, R., Stemann, L., and Bianchi, D.: Constraining the Ocean’s Biological Pump with in Situ Optical Observations and Supervised Learning. Part 1: Particle Size Distributions, <https://doi.org/10.1002/essoar.10509083.1>, <http://www.essoar.org/doi/10.1002/essoar.10509083.1>, 2021b.
- Cózar, A., Echevarría, F., González-Gordillo, J. I., Irigoien, X., Úbeda, B., Hernández-León, S., Palma, Á. T., Navarro, S., García-de Lomas, J., Ruiz, A., et al.: Plastic debris in the open ocean, *Proceedings of the National Academy of Sciences*, 111, 10 239–10 244, 2014.  
355



- de Madron, X. D., Radakovitch, O., Heussner, S., Loye-Pilot, M., and Monaco, A.: Role of the climatological and current variability on shelf-slope exchanges of particulate matter: Evidence from the Rhône continental margin (NW Mediterranean), *Deep Sea Research Part I: Oceanographic Research Papers*, 46, 1513–1538, 1999.
- de Madron, X. D., Ramondenc, S., Berline, L., Houpert, L., Bosse, A., Martini, S., Guidi, L., Conan, P., Curtil, C., Delsaut, N., et al.: Deep sediment resuspension and thick nepheloid layer generation by open-ocean convection, *Journal of Geophysical Research: Oceans*, 122, 2291–2318, 2017.
- 360 Duarte, C. M., Marbà, N., Gacia, E., Fourqurean, J. W., Beggins, J., Barrón, C., and Apostolaki, E. T.: Seagrass Community Metabolism: Assessing the Carbon Sink Capacity of Seagrass Meadows, *Global Biogeochemical Cycles*, 24, <https://doi.org/10.1029/2010GB003793>, 2010.
- 365 Fiedler, B., Grundle, D., Schütte, F., Karstensen, J., Löscher, C., Hauss, H., Wagner, H., Loginova, A. N., Kiko, R., Silva, P., et al.: Oxygen utilization and downward carbon flux in an oxygen-depleted eddy in the eastern tropical North Atlantic, *Biogeosciences (BG)*, 13, 5633–5647, 2016.
- Forest, A., Stemmann, L., Picheral, M., Burdorf, L., Robert, D., Fortier, L., and Babin, M.: Size distribution of particles and zooplankton across the shelf-basin system in southeast Beaufort Sea: combined results from an Underwater Vision Profiler and vertical net tows, *Biogeosciences*, 9, 1301, 2012.
- 370 Forest, A., Babin, M., Stemmann, L., Picheral, M., Sampei, M., Fortier, L., Gratton, Y., Bélanger, S. D., Sahlin, J., Doxaran, D., et al.: Ecosystem function and particle flux dynamics across the Mackenzie Shelf (Beaufort Sea, Arctic Ocean): an integrative analysis of spatial variability and biophysical forcings., *Biogeosciences*, 10, 2833–2866, 2013.
- German, C. and Von Damm, K.: Hydrothermal processes, *Treatise on geochemistry*, 6, 625, 2003.
- 375 Giering, S. L. C., Cavan, E. L., Basedow, S. L., Briggs, N., Burd, A. B., Darroch, L. J., Guidi, L., Irisson, J.-O., Iversen, M. H., Kiko, R., Lindsay, D., Marcolin, C. R., McDonnell, A. M. P., Möller, K. O., Passow, U., Thomalla, S., Trull, T. W., and Waite, A. M.: Sinking Organic Particles in the Ocean—Flux Estimates From in situ Optical Devices, *Frontiers in Marine Science*, 6, 834, <https://doi.org/10.3389/fmars.2019.00834>, <https://www.frontiersin.org/article/10.3389/fmars.2019.00834>, 2020.
- Gorsky, G., Picheral, M., and Stemmann, L.: Use of the Underwater Video Profiler for the study of aggregate dynamics in the North Mediterranean, *Estuarine, Coastal and Shelf Science*, 50, 121–128, 2000.
- 380 Gorsky, G., Prieur, L., Taupier-Letage, I., Stemmann, L., and Picheral, M.: Large particulate matter in the Western Mediterranean: I. LPM distribution related to mesoscale hydrodynamics, *Journal of Marine Systems*, 33, 289–311, 2002.
- Guidi, L., Gorsky, G., Claustre, H., Miquel, J., Picheral, M., and Stemmann, L.: Distribution and fluxes of aggregates > 100  $\mu\text{m}$  in the upper kilometer of the South-Eastern Pacific, *1foldr Import 2019-10-08 Batch 12*, 2008a.
- 385 Guidi, L., Jackson, G. A., Stemmann, L., Miquel, J. C., Picheral, M., and Gorsky, G.: Relationship between particle size distribution and flux in the mesopelagic zone, *Deep Sea Research Part I: Oceanographic Research Papers*, 55, 1364–1374, <https://doi.org/10.1016/j.dsr.2008.05.014>, <http://www.sciencedirect.com/science/article/pii/S0967063708001209>, 2008b.
- Guidi, L., Stemmann, L., Jackson, G. A., Ibanez, F., Claustre, H., Legendre, L., Picheral, M., and Gorsky, G.: Effects of phytoplankton community on production, size, and export of large aggregates: A world-ocean analysis, *Limnology and Oceanography*, 54, 1951–1963, 2009.
- 390 Guidi, L., Calil, P. H., Duhamel, S., Björkman, K. M., Doney, S. C., Jackson, G. A., Li, B., Church, M. J., Tozzi, S., Kolber, Z. S., et al.: Does eddy-eddy interaction control surface phytoplankton distribution and carbon export in the North Pacific Subtropical Gyre?, *Journal of Geophysical Research: Biogeosciences*, 117, 2012.



- Guidi, L., Legendre, L., Reygondeau, G., Uitz, J., Stemmann, L., and Henson, S. A.: A new look at ocean carbon remineraliza-  
395 tion for estimating deepwater sequestration, *Global Biogeochemical Cycles*, 29, 1044–1059, <https://doi.org/10.1002/2014GB005063>,  
<https://agupubs.onlinelibrary.wiley.com/doi/abs/10.1002/2014GB005063>, 2015.
- Hauss, H., Christiansen, S., Schütte, F., Kiko, R., Lima, M. E., Rodrigues, E., Karstensen, J., Löscher, C. R., Körtzinger, A., and Fiedler,  
B.: Dead zone or oasis in the open ocean? Zooplankton distribution and migration in low-oxygen medewater eddies, *Biogeosciences*, 13,  
1977–1989, <https://doi.org/10.5194/bg-13-1977-2016>, 2016.
- 400 Herman, A. W.: Design and calibration of a new optical plankton counter capable of sizing small zooplankton, *Deep Sea Research Part A.*  
*Oceanographic Research Papers*, 39, 395–415, 1992.
- Honjo, S., Doherty, K. W., Agrawal, Y. C., and Asper, V. L.: Direct optical assessment of large amorphous aggregates (marine snow) in the  
deep ocean, *Deep Sea Research Part A. Oceanographic Research Papers*, 31, 67–76, 1984.
- Jackson, G. A.: A model of the formation of marine algal flocs by physical coagulation processes, *Deep Sea Research Part A. Oceanographic*  
405 *Research Papers*, 37, 1197–1211, 1990.
- Jackson, G. A., Logan, B. E., Alldredge, A. L., and Dam, H. G.: Combining particle size spectra from a mesocosm experiment measured  
using photographic and aperture impedence (Coulter and Elzone) techniques, *Deep Sea Research Part II: Topical Studies in Oceanography*,  
42, 139–157, 1995.
- Jouandet, M.-P., Jackson, G. A., Carlotti, F., Picheral, M., Stemmann, L., and Blain, S.: Rapid formation of large aggregates during the spring  
410 bloom of Kerguelen Island: observations and model comparisons, *1foldr Import 2019-10-08 Batch 11*, 2014.
- Kalvelage, T., Lavik, G., Jensen, M. M., Revsbech, N. P., Löscher, C., Schunck, H., Desai, D. K., Hauss, H., Kiko, R., Holtappels, M.,  
LaRoche, J., Schmitz, R. A., Graco, M. I., and Kuypers, M. M. M.: Aerobic Microbial Respiration In Oceanic Oxygen Minimum Zones,  
*PLoS ONE*, 10, e0133 526, <https://doi.org/10.1371/journal.pone.0133526>, <http://dx.doi.org/10.1371%2Fjournal.pone.0133526>, 2015.
- Karthäuser, C., Ahmerkamp, S., Marchant, H. K., Bristow, L. A., Hauss, H., Iversen, M. H., Kiko, R., Maerz, J., Lavik, G.,  
415 and Kuypers, M. M. M.: Small Sinking Particles Control Anammox Rates in the Peruvian Oxygen Minimum Zone, 12, 3235,  
<https://doi.org/10.1038/s41467-021-23340-4>, <https://www.nature.com/articles/s41467-021-23340-4>, 2021.
- Katz, J., Donaghay, P., Zhang, J., King, S., and Russell, K.: Submersible holocamera for detection of particle characteristics and motions in  
the ocean, *Deep Sea Research Part I: Oceanographic Research Papers*, 46, 1455–1481, 1999.
- Kiko, R., Biastoch, A., Brandt, P., Cravatte, S., Hauss, H., Hummels, R., Kriest, I., Marin, F., McDonnell, A., Oshlies, A., et al.: Biological  
420 and physical influences on marine snowfall at the equator, *Nature Geoscience*, 10, 852–858, 2017.
- Kiko, R., Brandt, P., Christiansen, S., Faustmann, J., Kriest, I., Rodrigues, E., Schütte, F., and Hauss, H.: Zooplankton-Mediated Fluxes in  
the Eastern Tropical North Atlantic, *Frontiers in Marine Science*, 7, Art–Nr, 2020.
- Kiko, R., Picheral, M., Antoine, D., Babin, M., Berline, L., Biard, T., Boss, E., Brandt, P., Carlotti, F., Christiansen, S., Coppola, L., de la  
Cruz, L., Diamond-Riquier, E., de Madron, X. D., Elineau, A., Gorsky, G., Guidi, L., Hauss, H., Irisson, J.-O., Karp-Boss, L., Karstensen,  
425 J., gyun Kim, D., Lekanoff, R. M., Lombard, F., Lopes, R. M., Marec, C., McDonnell, A., Niemeyer, D., Noyon, M., O'Daly, S., Ohman,  
M., Pretty, J. L., Rogge, A., Searson, S., Shibata, M., Tanaka, Y., Tanhua, T., Taucher, J., Trudnowska, E., Turner, J. S., Waite, A. M.,  
and Stemmann, L.: The global marine particle size distribution dataset obtained with the Underwater Vision Profiler 5 - version 1, <https://doi.pangaea.de/10.1594/PANGAEA.924375>, 2021.
- Lampitt, R., Hillier, W., and Challenor, P.: Seasonal and diel variation in the open ocean concentration of marine snow aggregates, *Nature*,  
430 362, 737–739, 1993.



- Lombard, F., Boss, E., Waite, A. M., Vogt, M., Uitz, J., Stemann, L., Sosik, H. M., Schulz, J., Romagnan, J.-B., Picheral, M., Pearlman, J., Ohman, M. D., Niehoff, B., Möller, K. O., Miloslavich, P., Lara-Lpez, A., Kudela, R., Lopes, R. M., Kiko, R., Karp-Boss, L., Jaffe, J. S., Iversen, M. H., Irissou, J.-O., Fennel, K., Hauss, H., Guidi, L., Gorsky, G., Giering, S. L. C., Gaube, P., Gallagher, S., Dubelaar, G., Cowen, R. K., Carlotti, F., Briseño-Avena, C., Berline, L., Benoit-Bird, K., Bax, N., Batten, S., Ayata, S. D., Artigas, L. F., and Appeltans, W.: Globally Consistent Quantitative Observations of Planktonic Ecosystems, *Frontiers in Marine Science*, 6, <https://doi.org/10.3389/fmars.2019.00196>, <https://www.frontiersin.org/articles/10.3389/fmars.2019.00196/full>, 2019.
- Ludwig, W. and Probst, J.-L.: River sediment discharge to the oceans; present-day controls and global budgets, *American Journal of Science*, 298, 265–295, 1998.
- Many, G., de Madron, X. D., Verney, R., Bourrin, F., Renosh, P., Jourdin, F., and Gangloff, A.: Geometry, fractal dimension and settling velocity of flocs during flooding conditions in the Rhône ROFI, *Estuarine, Coastal and Shelf Science*, 219, 1–13, 2019.
- McCave, I.: Local and global aspects of the bottom nepheloid layers in the world ocean, *Netherlands Journal of Sea Research*, 20, 167–181, 1986.
- McCave, I. N.: Nepheloid layers, *Elements of physical oceanography: A derivative of the encyclopedia of ocean sciences*, pp. 0–282, 2009.
- Neal, E. G., Hood, E., and Smikrud, K.: Contribution of glacier runoff to freshwater discharge into the Gulf of Alaska, *Geophysical Research Letters*, 37, 2010.
- Niemeyer, D.: Modelling features of the biological pump and its impact on marine oxygen distribution, Ph.D. thesis, 2020.
- O’Hern, T. J., d’ Agostino, L., and Acosta, A. J.: Comparison of Holographic and Coulter Counter Measurements of Cavitation Nuclei in the Ocean, 110, 200–207, <https://doi.org/10.1115/1.3243535>, <https://doi.org/10.1115/1.3243535>.
- Picheral, M., Guidi, L., Stemann, L., Karl, D. M., Iddaoud, G., and Gorsky, G.: The Underwater Vision Profiler 5: An advanced instrument for high spatial resolution studies of particle size spectra and zooplankton, *Limnology and Oceanography: Methods*, 8, 462–473, 2010.
- Picheral, M. et al.: The Underwater Vision Profiler 6: an imaging sensor of particle size spectra and plankton, for autonomous and cabled platforms, *Limnology and Oceanography: Methods*, 2022.
- Puig, P., de Madron, X. D., Salat, J., Schroeder, K., Martín, J., Karageorgis, A. P., Palanques, A., Roullier, F., Lopez-Jurado, J. L., Emelianov, M., et al.: Thick bottom nepheloid layers in the western Mediterranean generated by deep dense shelf water cascading, *Progress in Oceanography*, 111, 1–23, 2013.
- Ratmeyer, V. and Wefer, G.: A high resolution camera system (ParCa) for imaging particles in the ocean: System design and results from profiles and a three-month deployment, *Journal of Marine Research*, 54, 589–603, 1996.
- Ratmeyer, V., Fischer, G., and Wefer, G.: Lithogenic particle fluxes and grain size distributions in the deep ocean off northwest Africa: Implications for seasonal changes of aeolian dust input and downward transport, *Deep Sea Research Part I: Oceanographic Research Papers*, 46, 1289–1337, 1999.
- Remsen, A., Hopkins, T. L., and Samson, S.: What You See Is Not What You Catch: A Comparison of Concurrently Collected Net, Optical Plankton Counter, and Shadowed Image Particle Profiling Evaluation Recorder Data from the Northeast Gulf of Mexico, 51, 129–151, <https://doi.org/10.1016/j.dsr.2003.09.008>, <http://www.sciencedirect.com/science/article/pii/S0967063703001614>, 2004.
- Roullier, F., Berline, L., Guidi, L., Durrieu De Madron, X., Picheral, M., Sciandra, A., Pesant, S., and Stemann, L.: Particle size distribution and estimated carbon flux across the Arabian Sea oxygen minimum zone, *Biogeosciences*, 11, 4541–4557, 2014.
- Sheldon, R. and Parsons, T.: A practical manual on the use of the Coulter Counter in marine science, Coulter Electronics, Toronto, 66, 1967.
- Stemann, L. and Boss, E.: Plankton and particle size and packaging: from determining optical properties to driving the biological pump, *Annual Review of Marine Science*, 4, 263–290, 2012.



- Stemmann, L., Picheral, M., and Gorsky, G.: Diel variation in the vertical distribution of particulate matter (> 0.15 mm) in the NW Mediter-  
470 ranean Sea investigated with the Underwater Video Profiler, *Deep Sea Research Part I: Oceanographic Research Papers*, 47, 505–531,  
2000.
- Stemmann, L., Gorsky, G., Marty, J.-C., Picheral, M., and Miquel, J.-C.: Four-year study of large-particle vertical distribution (0–1000  
m) in the NW Mediterranean in relation to hydrology, phytoplankton, and vertical flux, *Deep Sea Research Part II: Topical Studies in  
Oceanography*, 49, 2143–2162, 2002.
- 475 Stemmann, L., Jackson, G. A., and Ianson, D.: A vertical model of particle size distributions and fluxes in the midwater column that includes  
biological and physical processes—Part I: model formulation, *Deep Sea Research Part I: Oceanographic Research Papers*, 51, 865–884,  
2004.
- Stemmann, L., Eloire, D., Sciandra, A., Jackson, G., Guidi, L., Picheral, M., and Gorsky, G.: Volume distribution for particles between 3.5  
to 2000  $\mu\text{m}$  in the upper 200 m region of the South Pacific Gyre, *Biogeosciences*, 5, 299–310, 2008a.
- 480 Stemmann, L., Prieur, L., Legendre, L., Taupier-Letage, I., Picheral, M., Guidi, L., and Gorsky, G.: Effects of frontal processes on marine  
aggregate dynamics and fluxes: An interannual study in a permanent geostrophic front (NW Mediterranean), *Journal of Marine Systems*,  
70, 1–20, 2008b.
- Stemmann, L., Youngbluth, M., Robert, K., Hosia, A., Picheral, M., Paterson, H., Ibanez, F., Guidi, L., Lombard, F., and Gorsky, G.: Global  
zoogeography of fragile macrozooplankton in the upper 100–1000 m inferred from the underwater video profiler, *ICES Journal of Marine  
485 Science*, 65, 433–442, 2008c.
- Stemmann, L., Picheral, M., Guidi, L., Lombard, F., Prejger, F., Claustre, H., and Gorsky, G.: Assessing the spatial and temporal distributions  
of zooplankton and marine particles using the Underwater Vision Profiler, *Sensors for ecology*, p. 119, 2012.
- Suzuki, N. and Kato, K.: Studies on suspended materials marine snow in the sea: Part . sources of marine snow, *Bulletin of the Faculty of  
Fisheries of Hokkaido University*, 4, 132–137, 1953.
- 490 Thomsen, S., Karstensen, J., Kiko, R., Krahnemann, G., Dengler, M., and Engel, A.: Remote and local drivers of oxygen and nitrate variability  
in the shallow oxygen minimum zone off Mauritania in June 2014, *Biogeosciences*, 16, 979–998, 2019.
- Trudnowska, E., Lacour, L., Ardyna, M., Rogge, A., Irisson, J. O., Waite, A. M., Babin, M., and Stemmann, L.: Marine Snow  
Morphology Illuminates the Evolution of Phytoplankton Blooms and Determines Their Subsequent Vertical Export, 12, 2816,  
<https://doi.org/10.1038/s41467-021-22994-4>, <https://www.nature.com/articles/s41467-021-22994-4>, 2021.
- 495 Vilgrain, L., Maps, F., Picheral, M., Babin, M., Aubry, C., Irisson, J.-O., and Ayata, S.-D.: Trait-Based Approach Using in Situ Copepod  
Images Reveals Contrasting Ecological Patterns across an Arctic Ice Melt Zone, 66, 1155–1167, <https://doi.org/10.1002/lno.11672>, <https://aslopubs.onlinelibrary.wiley.com/doi/abs/10.1002/lno.11672>, 2021.
- Waite, A. M., Stemmann, L., Guidi, L., Calil, P. H., Hogg, A. M. C., Feng, M., Thompson, P. A., Picheral, M., and Gorsky, G.: The wineglass  
effect shapes particle export to the deep ocean in mesoscale eddies, *Geophysical Research Letters*, 43, 9791–9800, 2016.
- 500 Weber, T. and Bianchi, D.: Efficient Particle Transfer to Depth in Oxygen Minimum Zones of the Pacific and Indian Oceans, *Frontiers in  
Earth Science*, 8, <https://doi.org/10.3389/feart.2020.00376>, 2020.
- Wiebe, P. H. and Benfield, M. C.: From the Hensen net toward four-dimensional biological oceanography, *Progress in Oceanography*, 56,  
7–136, 2003.
- Zhou, M.: What Determines the Slope of a Plankton Biomass Spectrum?, 28, 437–448, <https://doi.org/10.1093/plankt/fbi119>, <https://doi.org/10.1093/plankt/fbi119>.
- 505



<https://doi.org/10.5194/essd-2022-51>  
Preprint. Discussion started: 12 April 2022  
© Author(s) 2022. CC BY 4.0 License.



Zuniga, D., Calafat, A., Heussner, S., Miserocchi, S., Sanchez-Vidal, A., Garcia-Orellana, J., Canals, M., Sánchez-Cabeza, J., Carbonne, J., Delsaut, N., et al.: Compositional and temporal evolution of particle fluxes in the open Algero–Balearic basin (Western Mediterranean), *Journal of Marine Systems*, 70, 196–214, 2008.



**Tables**

**510 Table 1**

Table 1: Geospatial information for UVP projects.

UVP project name	Ecopart ID	Profiles	Time period	Latitude range	Longitude range	UVP manager(s)
uvp5_sn000_boum2008	2	184	2008-06-19 to 2008-07-18	43.21 to 33.47	32.77 to 4.93	L Stemmman, M Picheral
uvp5_sn000_ccelter_2012	3	62	2012-07-28 to 2012-08-21	34.6 to 33.1	-118.31 to -123.69	L Stemmman, M Picheral
uvp5_sn000_lohafex2009	4	57	2009-01-16 to 2009-03-06	-47.58 to -50.01	-13.64 to -35.26	L Stemmman, M Picheral
uvp5_sn000_iter2008	5	75	2008-09-30 to 2008-10-28	34.2 to 32.15	-117.96 to -124.0	L Stemmman, M Picheral
uvp5_sn000_malina2009	16	154	2009-07-18 to 2009-08-22	72.06 to 69.47	-126.48 to -140.81	L Stemmman, M Picheral
uvp5_sn000_msm049	19	22	2015-11-30 to 2015-12-19	20.32 to 12.0	-20.5 to -24.28	R Kiko, H Hauss
uvp5_sn000_operex2008	20	92	2008-07-31 to 2008-08-12	25.75 to 22.24	-156.25 to -160.67	L Guidi, L Stemmman
uvp5_sn000_tara2009	6	46	2009-10-11 to 2009-12-15	43.36 to 33.37	35.33 to 7.89	L Stemmman, M Picheral
uvp5_sn000_tara2010	7	196	2010-01-09 to 2010-12-17	27.16 to -55.1	73.91 to -65.91	L Stemmman, M Picheral
uvp5_sn000_tara2011	99	264	2011-01-03 to 2011-12-21	35.42 to -64.36	-53.01 to -159.06	L Stemmman, M Picheral
uvp5_sn000_tara2012	9	32	2012-01-28 to 2012-02-18	39.24 to 32.92	-66.54 to -75.07	L Stemmman, M Picheral
uvp5_sn001_2012_moosse_ge	21	87	2012-07-24 to 2012-08-08	43.9 to 40.0	9.64 to 3.44	L Stemmman, M Picheral
uvp5_sn001_2012_msm22	22	113	2012-10-24 to 2012-11-22	18.5 to -5.01	-19.68 to -26.99	R Kiko, H Hauss
uvp5_sn001_2012_msm23	23	64	2012-11-26 to 2012-12-16	17.6 to -18.19	1.0 to -24.3	R Kiko, H Hauss
uvp5_sn001_2013_m92	24	30	2013-01-19 to 2013-01-30	-11.0 to -12.61	-77.17 to -78.63	R Kiko, H Hauss
uvp5_sn001_2013_m93	25	148	2013-02-08 to 2013-03-04	-12.16 to -13.97	-76.42 to -78.42	R Kiko, H Hauss
uvp5_sn001_2013_m96	26	77	2013-05-02 to 2013-05-22	17.7 to 11.33	-20.08 to -60.3	R Kiko, H Hauss
uvp5_sn001_2013_m97	27	180	2013-05-26 to 2013-06-23	17.57 to 8.0	-17.75 to -24.28	R Kiko, H Hauss
uvp5_sn001_2013_m98	28	52	2013-07-02 to 2013-07-23	-5.12 to -11.5	13.5 to -35.89	R Kiko, H Hauss
uvp5_sn001_2014_msm40	29	5	2014-08-17 to 2014-08-19	59.54 to 59.19	-39.74 to -43.54	R Kiko, H Hauss
uvp5_sn002_iado_2014	251	26	2014-09-20 to 2014-09-23	43.69 to 43.37	7.89 to 7.14	J-O Irissou
uvp5_sn002_iado_2015	252	36	2015-09-16 to 2015-09-20	43.65 to 43.42	7.8 to 7.13	J-O Irissou
uvp5_sn002_iado_2016	30	16	2016-09-18 to 2016-09-21	43.67 to 43.39	7.6 to 7.31	J-O Irissou
uvp5_sn002_iado_2018	121	10	2018-09-22 to 2018-09-23	43.59 to 43.31	7.68 to 7.39	J-O Irissou
uvp5_sn002_moosse_dyf_2013	10	4	2013-09-14 to 2013-10-24	43.42 to 43.42	7.9 to 7.9	L Stemmman, M Picheral
uvp5_sn002_moosse_dyf_2014	11	9	2014-03-11 to 2014-12-10	43.68 to 43.36	7.9 to 7.31	L Stemmman, M Picheral
uvp5_sn002_moosse_dyf_2015	12	9	2015-02-08 to 2015-12-10	43.44 to 43.42	7.87 to 7.82	L Stemmman, M Picheral
uvp5_sn002_moosse_dyf_2016	13	10	2016-02-05 to 2016-12-10	43.43 to 43.41	7.87 to 7.86	L Guidi
uvp5_sn002_moosse_dyf_2017	14	8	2017-02-07 to 2017-11-08	43.43 to 43.41	7.88 to 7.86	L Coppola
uvp5_sn002_moosse_dyf_2018	166	4	2018-01-23 to 2018-08-27	43.42 to 43.41	7.87 to 7.85	L Guidi
uvp5_sn002_moosse_ge_2013	15	6	2013-06-11 to 2013-06-15	43.75 to 43.41	9.36 to 7.52	L Stemmman, M Picheral



17	uwp5_sn002_moose_ge_2014	84	2014-07-04 to 2014-07-20	43.93 to 40.0	9.72 to 3.5	L Stemmann, M Picheral
31	uwp5_sn002_moose_ge_2015_filtered	72	2015-07-10 to 2015-07-27	43.88 to 40.0	9.63 to 3.54	L Stemmann, M Picheral
18	uwp5_sn002_moose_ge_2016_filtered	84	2016-05-19 to 2016-06-09	43.63 to 40.0	8.92 to 3.54	L Guidi
100	uwp5_sn002_moose_ge_2017_filtered	116	2017-08-31 to 2017-09-23	43.88 to 39.99	9.63 to 3.5	L Coppola
149	uwp5_sn002_moose_ge_2019	88	2019-06-08 to 2019-07-01	43.88 to 40.0	9.63 to 3.5	L Coppola
32	uwp5_sn002_somba_ge_2014	65	2014-08-17 to 2014-09-08	39.72 to 36.55	9.48 to -0.7	L Stemmann, M Picheral
33	uwp5_sn002zd_cascade2011	82	2011-03-02 to 2011-03-21	43.4 to 41.13	6.13 to 3.36	X. Durrieu de Madron
34	uwp5_sn002zd_ccelter_2011	58	2011-06-27 to 2011-07-16	34.11 to 32.58	-120.85 to -121.78	L Stemmann, M Picheral
35	uwp5_sn002zd_gatekeeper2010	21	2010-07-11 to 2010-07-14	36.8 to 36.7	-121.97 to -122.58	L Stemmann, M Picheral
36	uwp5_sn002zd_keops2	106	2011-10-14 to 2011-11-20	-45.0 to -50.65	75.0 to 52.1	L Stemmann, M Picheral
36	uwp5_sn002zd_keops2	106	2011-10-14 to 2011-11-20	-45.0 to -50.65	75.0 to 52.1	L Stemmann, M Picheral
37	uwp5_sn002zd_omer	10	2012-04-08 to 2012-04-09	43.61 to 43.58	7.58 to 7.49	L Stemmann, M Picheral
38	uwp5_sn002zd_omer_2	7	2012-05-20 to 2012-05-22	43.69 to 43.69	7.32 to 7.31	L Stemmann, M Picheral
40	uwp5_sn003_2015_kaxis	3	2016-01-21 to 2016-01-23	-61.97 to -62.7	95.37 to 91.53	L Stemmann, M Picheral
41	uwp5_sn003_cassiopee_2015	82	2015-07-20 to 2015-08-15	2.0 to -19.98	168.01 to 148.05	L Stemmann, M Picheral
42	uwp5_sn003_ccelter_2014	62	2014-08-07 to 2014-09-02	34.87 to 32.28	-118.28 to -123.9	L Stemmann, M Picheral
42	uwp5_sn003_ccelter_2014	62	2014-08-07 to 2014-09-02	34.87 to 32.28	-118.28 to -123.9	L Stemmann, M Picheral
43	uwp5_sn003_ccelter_2016	60	2016-04-20 to 2016-05-11	35.09 to 32.7	-117.36 to -123.21	T Biard
144	uwp5_sn003_esiro_iioc	52	2019-05-15 to 2019-06-09	-11.45 to -39.49	113.42 to 109.88	D Antoine
44	uwp5_sn003_dewex_spring_2013	83	2013-04-05 to 2013-04-19	43.63 to 40.08	8.64 to 3.51	L Stemmann, M Picheral
90	uwp5_sn003_iado_2017	24	2017-09-22 to 2017-09-24	43.67 to 43.35	7.65 to 7.31	J-O Irsson
1	uwp5_sn003_jerico_2017	27	2017-07-10 to 2017-07-16	59.85 to 54.97	24.84 to 10.5	L Stemmann, M Picheral
124	uwp5_sn003_mobydick_2018	61	2018-02-21 to 2018-03-19	-29.04 to -52.6	74.9 to 59.06	L Guidi
46	uwp5_sn003_outpace_2015	205	2015-02-21 to 2015-03-31	-17.9 to -22.0	178.64 to -178.51	L Guidi
47	uwp5_sn003_sargasso_a	52	2014-03-16 to 2014-04-05	31.5 to 24.67	-62.48 to -68.56	F Lombard
48	uwp5_sn003_sargasso_b	32	2014-04-09 to 2014-04-22	35.18 to 25.67	-31.63 to -59.52	F Lombard
49	uwp5_sn003_tara2013	155	2013-05-26 to 2013-10-27	79.67 to 54.41	174.99 to -168.66	L Stemmann, M Picheral
50	uwp5_sn003zp_pelgas2012	34	2012-05-26 to 2012-06-03	46.11 to 44.86	-1.27 to -2.6	L Stemmann, M Picheral
51	uwp5_sn003zp_tara2012	77	2011-12-30 to 2012-03-26	44.36 to 9.84	-10.07 to -88.49	L Stemmann, M Picheral
52	uwp5_sn005_batman	6	2016-03-11 to 2016-03-15	42.8 to 42.8	6.08 to 6.08	F Carlotti, Leo Bertine
53	uwp5_sn005_dewex_2013_winter	53	2013-02-03 to 2013-02-18	42.88 to 40.08	8.59 to 3.45	L Stemmann, M Picheral
54	uwp5_sn005_dy032_2015_filtered	15	2015-06-24 to 2015-07-03	49.08 to 48.68	-16.26 to -17.06	F Carlotti, Leo Bertine
55	uwp5_sn005_moose_ge_2013	39	2013-06-29 to 2013-07-07	43.05 to 39.96	8.0 to 3.39	L Stemmann, M Picheral
152	UVPsn008_2018_leg02c	42	2018-07-25 to 2018-08-13	71.41 to 59.22	-48.46 to -70.18	M Babin, M Picheral
56	uwp5_sn008_an1304	101	2013-07-29 to 2013-09-15	81.28 to 53.8	-55.43 to -116.96	M Babin, M Picheral
57	uwp5_sn008_an1405	64	2014-07-27 to 2014-08-13	81.37 to 68.68	-57.88 to -108.51	M Babin, M Picheral
58	uwp5_sn008_an1406	82	2014-08-17 to 2014-09-23	75.21 to 69.37	-123.03 to -169.83	M Babin, M Picheral
59	uwp5_sn008_an1407	11	2014-09-30 to 2014-10-08	71.12 to 53.8	-55.44 to -72.26	M Babin, M Picheral



uwp5_sn008_green_2015_icecamp	60	32	2015-04-18 to 2015-06-21	67.48 to 67.48	-63.79 to -63.79	M Babin, M Picheral
uwp5_sn008_green_2016_icecamp	61	29	2016-03-02 to 2016-07-04	67.48 to 67.48	-63.79 to -63.79	M Babin, M Picheral
uwp5_sn008_ips_amundsen_2018	105	7	2018-07-16 to 2018-07-22	69.29 to 67.24	-60.39 to -64.64	M Babin, M Picheral
uwp5_sn008_subice_2014	62	228	2014-05-15 to 2014-06-20	73.27 to 63.95	-162.0 to -168.95	L Stemmann, M Picheral
uwp5_sn008_uvp_azomp	161	35	2019-06-01 to 2019-06-17	60.57 to 44.27	-48.23 to -63.32	A.M.P. McDonnell
uwp5_sn009_pomz	132	29	2016-12-27 to 2017-01-13	21.36 to 14.0	-104.63 to -107.83	A.M.P. McDonnell
uwp5_sn009_en_534_mcdonnell	257	10	2013-10-24 to 2013-10-27	39.81 to 38.38	-71.01 to -72.91	A.M.P. McDonnell
uwp5_sn009_2015_goa	63	70	2015-07-17 to 2015-07-30	60.3 to 54.64	-132.86 to -149.47	A.M.P. McDonnell, J.S. Turner
uwp5_sn009_2015_p16n	64	171	2015-04-11 to 2015-06-18	56.29 to -16.96	-149.86 to -153.23	A.M.P. McDonnell
uwp5_sn009_2015_p16n_goa	65	15	2015-06-19 to 2015-06-23	56.79 to 54.35	-135.95 to -149.14	A.M.P. McDonnell, J.S. Turner
uwp5_sn009_2016_goa_fall	146	37	2016-09-16 to 2016-09-21	61.08 to 57.8	-146.75 to -149.48	A.M.P. McDonnell
uwp5_sn009_2016_goa_spring	141	33	2016-04-30 to 2016-05-27	60.99 to 57.79	-147.08 to -149.49	A.M.P. McDonnell
uwp5_sn009_2017_asgard	112	71	2017-06-09 to 2017-06-27	69.04 to 63.3	-164.43 to -172.59	A.M.P. McDonnell
uwp5_sn009_2017_sewardline_fall	142	49	2017-09-16 to 2017-09-22	60.99 to 57.79	-146.98 to -149.49	A.M.P. McDonnell
uwp5_sn009_2018_asgard_filtered	234	69	2018-06-06 to 2018-06-24	69.45 to 61.29	-164.43 to -171.51	A.M.P. McDonnell
uwp5_sn009_2018_nga_fall_filtered	131	60	2018-09-12 to 2018-09-21	60.25 to 57.21	-145.5 to -151.39	A.M.P. McDonnell
uwp5_sn009_2019_nga_iter_spring_filtered	139	54	2019-04-30 to 2019-05-08	60.83 to 56.97	-147.39 to -151.58	A.M.P. McDonnell
uwp5_sn009_2019_nga_iter_summer_filtered	151	57	2019-06-29 to 2019-07-17	60.53 to 56.66	-144.59 to -151.59	A.M.P. McDonnell
uwp5_sn009_2019_nga_iter_summer_filtered	151	57	2019-06-29 to 2019-07-17	60.53 to 56.66	-144.59 to -151.59	A.M.P. McDonnell
uwp5_sn009_2019_nga_iter_summer_filtered	147	21	2016-07-08 to 2016-08-02	78.35 to 71.6	-158.48 to -164.06	A.M.P. McDonnell
uwp5_sn009_chukchi_borderlands_2016	104	70	2018-04-19 to 2018-05-04	61.25 to 57.79	-143.89 to -149.47	A.M.P. McDonnell
uwp5_sn009_2018_nga_spring_filtered	66	10	2014-09-13 to 2014-09-16	59.84 to 58.24	-147.93 to -149.49	A.M.P. McDonnell
uwp5_sn009_sewardline_f2014	148	24	2014-08-20 to 2014-08-28	70.62 to 69.72	-140.3 to -145.11	A.M.P. McDonnell
uwp5_sn009_tb14	67	9	2014-05-03 to 2014-05-05	59.84 to 58.68	-148.35 to -149.48	A.M.P. McDonnell
uwp5_sn009_txs14	109	6	2014-02-14 to 2014-03-07	19.51 to 16.75	-24.3 to -25.12	R Kiko, H Hauss
uwp5_sn010_2014_eddy	68	138	2014-03-18 to 2014-04-14	19.23 to 7.0	-17.5 to -26.0	R Kiko, H Hauss
uwp5_sn010_2014_m105	69	115	2014-04-19 to 2014-05-24	17.6 to -11.5	-21.21 to -35.89	R Kiko, H Hauss
uwp5_sn010_2014_m106	70	73	2014-06-05 to 2014-06-29	19.9 to 11.45	-16.32 to -23.0	R Kiko, H Hauss
uwp5_sn010_2014_m107	71	12	2014-07-09 to 2014-07-20	49.0 to 39.52	-15.96 to -16.52	R Kiko, H Hauss
uwp5_sn010_2014_m108	72	39	2014-11-04 to 2014-11-15	21.21 to -1.0	-21.12 to -24.29	R Kiko, H Hauss
uwp5_sn010_2014_ps88b	73	82	2015-05-02 to 2015-06-02	17.58 to 5.0	-18.0 to -57.67	R Kiko, H Hauss
uwp5_sn010_2015_m116	74	49	2015-09-08 to 2015-09-26	17.61 to -5.0	-21.21 to -24.33	R Kiko, H Hauss
uwp5_sn010_2015_m119	75	8	2015-10-31 to 2015-11-02	-6.21 to -10.59	13.43 to 11.38	R Kiko, H Hauss
uwp5_sn010_2015_m120	76	88	2015-11-22 to 2015-12-24	-3.0 to -29.58	15.56 to -0.01	R Kiko, H Hauss
uwp5_sn010_2015_m121	226	43	2016-03-30 to 2016-04-07	68.27 to 67.78	14.7 to 14.04	H Hauss, R Kiko
uwp5_sn010_2016_love	77	112	2016-08-29 to 2016-10-01	17.7 to -11.5	-19.0 to -35.89	R Kiko, H Hauss
uwp5_sn010_2016_m130	223	89	2016-10-08 to 2016-11-09	-6.21 to -23.0	14.37 to -32.0	R Kiko, H Hauss
uwp5_sn010_2016_m131	110	72	2017-07-14 to 2017-08-08	23.0 to 17.5	-17.64 to -26.0	R Kiko



uwp5_sn010_2017_fluxes2	111	53	2017-11-02 to 2017-11-20	27.67 to 20.39	-15.82 to -20.65	R Kiko
uwp5_sn010_2017_m135	95	141	2017-03-02 to 2017-04-07	-10.67 to -31.03	-70.3 to -86.0	R Kiko, H Hauss
uwp5_sn010_2017_m136	96	98	2017-04-12 to 2017-05-02	-12.19 to -15.51	-76.47 to -78.5	R Kiko, H Hauss
uwp5_sn010_2017_m137	97	85	2017-05-06 to 2017-05-27	-12.1 to -12.98	-77.06 to -78.19	R Kiko, H Hauss
uwp5_sn010_2017_m138	98	42	2017-06-03 to 2017-06-29	1.5 to -16.25	-75.43 to -85.84	R Kiko, H Hauss
uwp5_sn010_2018_m145	172	89	2018-02-13 to 2018-03-12	17.61 to -11.5	-21.23 to -35.89	R Kiko, H Hauss
uwp5_sn010_2018_m147	171	4	2018-05-01 to 2018-05-04	3.95 to 1.91	-46.44 to -48.26	R Kiko, H Hauss
uwp5_sn010_2018_m148	173	92	2018-05-30 to 2018-06-28	-6.21 to -22.67	14.21 to -35.88	R Kiko, H Hauss
uwp5_sn011_2016_syTUMSAT1	246	2	2016-09-26 to 2016-09-27	35.06 to 35.06	138.78 to 138.68	Y. Tanaka
uwp5_sn011_2017_syTUMSAT2	247	10	2017-05-22 to 2017-05-24	35.1 to 33.4	139.87 to 139.41	Y. Tanaka
uwp5_sn200_ilhas_2017_filtered	240	38	2017-02-02 to 2017-02-13	-20.06 to -21.14	-28.3 to -40.25	R. Lopes
uwp5_sn200_moose_ge_2018_filtered	168	32	2018-05-27 to 2018-06-05	43.0 to 40.0	7.98 to 3.82	L Coppola
uwp5_sn200_perle_02_2019_filtered	235	31	2019-02-27 to 2019-03-04	35.95 to 34.04	25.3 to 22.96	X. D. de Madron
uwp5_sn200_perle_02_2019_filtered	235	31	2019-02-27 to 2019-03-04	35.95 to 34.04	25.3 to 22.96	X. D. de Madron
uwp5_sn201_2015_naames_01	80	26	2015-11-14 to 2015-11-25	54.11 to 40.51	-37.51 to -40.48	L. Karp-Boss, E. Boss
uwp5_sn201_2016_naames_02	81	42	2016-05-17 to 2016-05-29	56.34 to 44.05	-38.21 to -46.15	L. Karp-Boss, E. Boss
uwp5_sn201_2017_naames_03	92	40	2017-09-04 to 2017-09-17	53.4 to 42.38	-39.13 to -48.95	L. Karp-Boss, E. Boss
uwp5_sn201_2018_naames_04_filtered	236	12	2018-03-27 to 2018-04-01	44.48 to 39.28	-38.28 to -43.53	L. Karp-Boss, E. Boss
uwp5_sn201_ccelter_2017	83	90	2017-06-01 to 2017-07-01	35.58 to 33.02	-118.11 to -123.18	T Biard
uwp5_sn201_ccelter_2019_filtered	154	77	2019-08-06 to 2019-09-05	36.45 to 32.86	-117.66 to -125.07	T Biard
uwp5_sn201_exports01_filtered	228	84	2018-08-14 to 2018-09-09	50.6 to 49.93	-144.35 to -145.22	L. Karp-Boss, E. Boss
uwp5_sn202_msm060_filtered	231	127	2017-01-04 to 2017-01-31	-34.04 to -34.83	18.15 to -51.83	A. Rogge
uwp5_sn202_msm074_filtered	232	114	2018-05-25 to 2018-06-19	60.4 to 47.55	-36.1 to -54.0	A. Rogge
uwp5_sn202_ps99_20_06_filtered	237	8	2016-06-20 to 2016-06-20	74.93 to 74.7	18.15 to 17.36	A. Rogge
uwp5_sn202_ps99_21_06_3_filtered	85	27	2016-06-22 to 2016-07-12	79.59 to 77.59	11.09 to -5.41	A. Rogge
uwp5_sn203_greenedge_2016	86	86	2016-06-05 to 2016-06-22	69.03 to 50.34	-52.84 to -63.2	L. Stemmann, M. Picheral
uwp5_sn203_greenedge_2016_1b	87	110	2016-06-24 to 2016-07-10	70.51 to 68.02	-56.9 to -63.28	L. Stemmann, M. Picheral
uwp5_sn205_coastdark_2019	153	38	2019-07-26 to 2019-08-11	79.04 to 76.64	16.87 to 7.76	E. Trudnowska
uwp5_sn205_perle_02_2019_filtered	134	81	2019-03-04 to 2019-03-16	35.88 to 33.54	28.81 to 24.38	X. D. de Madron
uwp5_sn205_perle_03_2020_filtered	238	21	2020-03-13 to 2020-03-16	42.94 to 39.19	14.26 to 9.59	X. D. de Madron
uwp5_sn207_2018_exports_np_sr1812_filtered	230	134	2018-08-11 to 2018-09-09	51.04 to 49.43	-131.54 to -145.76	A.M.P. McDonnell
uwp5_sn207_2018_s04p_filtered	150	111	2018-03-13 to 2018-05-09	-59.06 to -75.29	179.42 to -179.29	A.M.P. McDonnell
uwp5hd_sn207_2019_i06s_tcn322_filtered	138	44	2019-04-16 to 2019-05-11	-33.23 to -68.35	31.53 to 28.09	A.M.P. McDonnell
uwp5_sn210_2018_msm080	270	127	2018-12-27 to 2019-01-25	-8.5 to -16.4	-74.17 to -81.0	R Kiko, H Hauss
uwp5_sn210_2019_m156	271	57	2019-07-04 to 2019-07-29	21.44 to 17.58	-16.39 to -24.33	R Kiko, H Hauss
uwp5_sn210_2019_m157	272	24	2019-08-21 to 2019-09-13	-17.26 to -25.0	14.56 to 11.07	R Kiko, H Hauss
uwp5_sn210_2019_m159	256	46	2019-11-02 to 2019-11-18	17.6 to -11.5	-24.25 to -35.02	R Kiko, H Hauss
uwp5_sn210_2019_m160	275	71	2019-11-24 to 2019-12-17	18.6 to 14.27	-19.7 to -25.99	R Kiko, H Hauss



R Kiko, H Hauss  
Margaux Noyon

-50.83 to -60.08  
26.29 to 25.7

14.03 to 7.25  
-33.73 to -34.03

2020-01-18 to 2020-02-16  
2020-10-28 to 2020-11-23

46  
36

273  
268

uwp5\_sn210\_2020\_msm089  
uwp5\_sn221\_algoa\_bay\_2020



## Table 2

Table 2: References for datasets published before the revision of the inter-calibration procedure.

	UVP project name	Link to previously published UVP particle dataset
	uvp5_sn000_tara2009	<a href="https://doi.pangaea.de/10.1594/PANGAEA.836321">https://doi.pangaea.de/10.1594/PANGAEA.836321</a>
	uvp5_sn000_tara2010	<a href="https://doi.pangaea.de/10.1594/PANGAEA.836321">https://doi.pangaea.de/10.1594/PANGAEA.836321</a>
	uvp5_sn000_tara2011	<a href="https://doi.pangaea.de/10.1594/PANGAEA.836321">https://doi.pangaea.de/10.1594/PANGAEA.836321</a>
	uvp5_sn000_tara2012	<a href="https://doi.pangaea.de/10.1594/PANGAEA.836321">https://doi.pangaea.de/10.1594/PANGAEA.836321</a>
	uvp5_sn003_tara2013	<a href="https://doi.pangaea.de/10.1594/PANGAEA.836321">https://doi.pangaea.de/10.1594/PANGAEA.836321</a>
	uvp5_sn003zp_tara2012	<a href="https://doi.pangaea.de/10.1594/PANGAEA.836321">https://doi.pangaea.de/10.1594/PANGAEA.836321</a>
	uvp5_sn001_2012_msm22	<a href="https://doi.org/10.1594/PANGAEA.874871">https://doi.org/10.1594/PANGAEA.874871</a>
515	uvp5_sn001_2012_msm23	<a href="https://doi.pangaea.de/10.1594/PANGAEA.846229">https://doi.pangaea.de/10.1594/PANGAEA.846229</a>
	uvp5_sn001_2013_m92	<a href="https://doi.org/10.1594/PANGAEA.885756">https://doi.org/10.1594/PANGAEA.885756</a>
	uvp5_sn001_2013_m96	<a href="https://doi.pangaea.de/10.1594/PANGAEA.846153">https://doi.pangaea.de/10.1594/PANGAEA.846153</a>
	uvp5_sn010_2014_m106	<a href="https://doi.org/10.1594/PANGAEA.874870">https://doi.org/10.1594/PANGAEA.874870</a>
	uvp5_sn010_2014_m107	<a href="https://doi.org/10.1594/PANGAEA.885759">https://doi.org/10.1594/PANGAEA.885759</a>
	uvp5_sn010_2015_m119	<a href="https://doi.org/10.1594/PANGAEA.874872">https://doi.org/10.1594/PANGAEA.874872</a>
	uvp5_sn003_cassiopee_2015	<a href="https://doi.org/10.1594/PANGAEA.876216">https://doi.org/10.1594/PANGAEA.876216</a>
	uvp5_sn009_2015_p16n	<a href="https://doi.org/10.1594/PANGAEA.874875">https://doi.org/10.1594/PANGAEA.874875</a>
	uvp5_sn202_ps99_21_06_3_filtered	<a href="https://doi.pangaea.de/10.1594/PANGAEA.896047">https://doi.pangaea.de/10.1594/PANGAEA.896047</a>

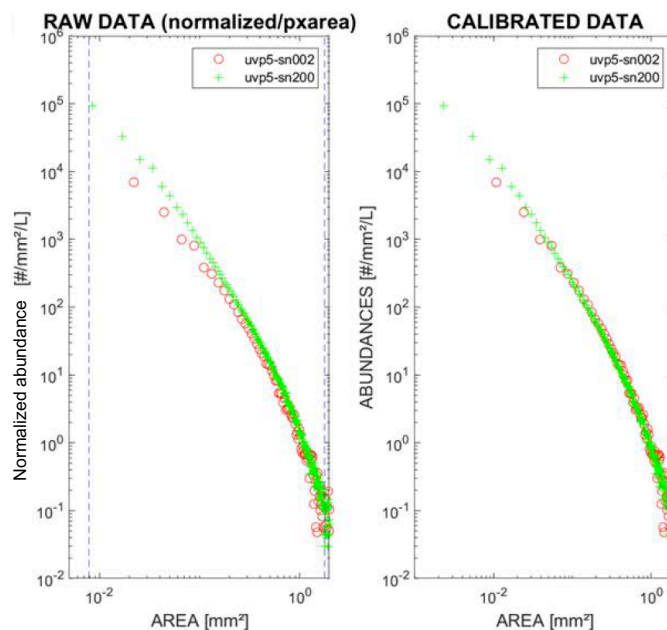


**Figure 1.** UVP5 inter-calibration procedure based on the normalized size spectrum. To calculate the normalized size spectrum, the abundance of particles in a given size class is divided by the mean area of the size class. Normalized abundance of each size class is then plotted against the area of the size class. Figure 1a shows the raw number size spectrum data of the unit to be adjusted (sn200) for one exemplary inter-calibration experiment against sn002 and Fig 1b the respective data after adjustment of the parameters  $A_a$  and  $Exp$  to coincide better with the number size spectrum of UVP5 sn002.

## Figures



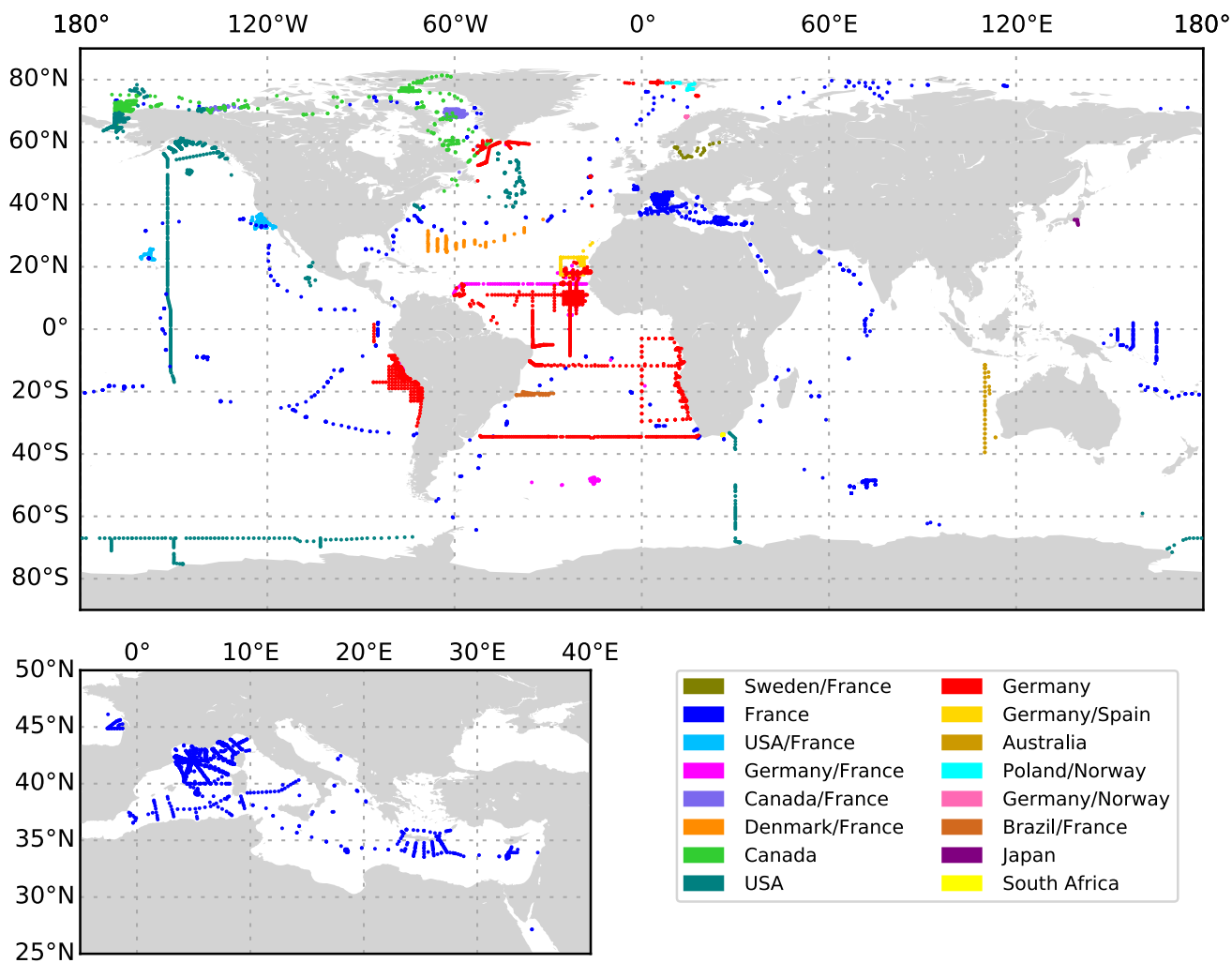


**Figure 2.** Global distribution of UVP5 data. Lower left panel shows the data distribution in the Mediterranean Sea.

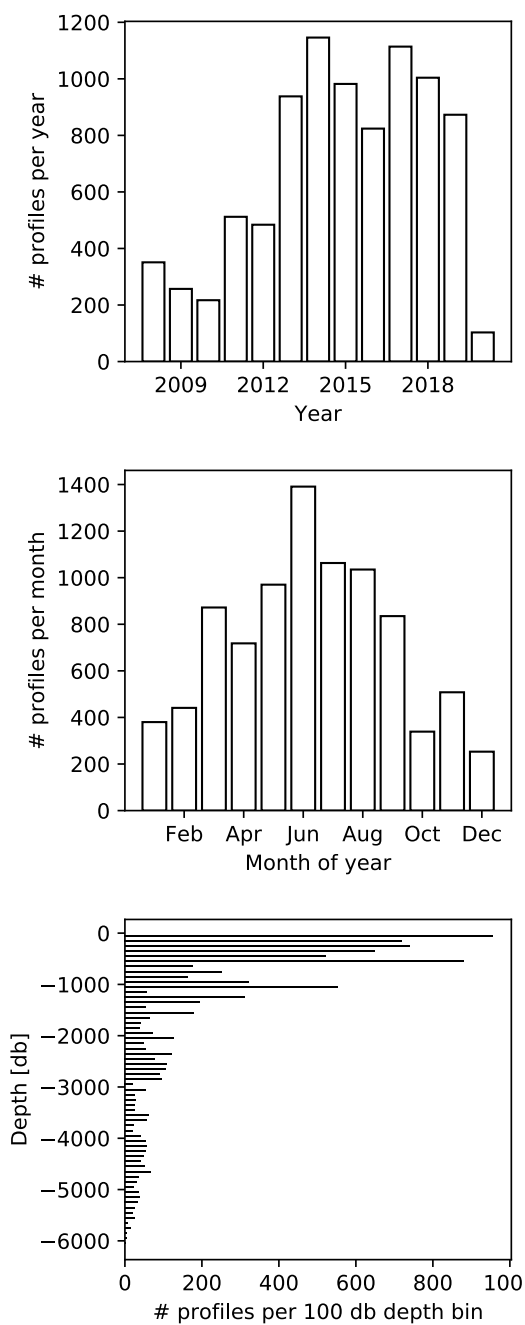


**Figure 3.** UVP5 data distribution per year, month and maximum profile depth (aggregated in 100 dbar depth bins).

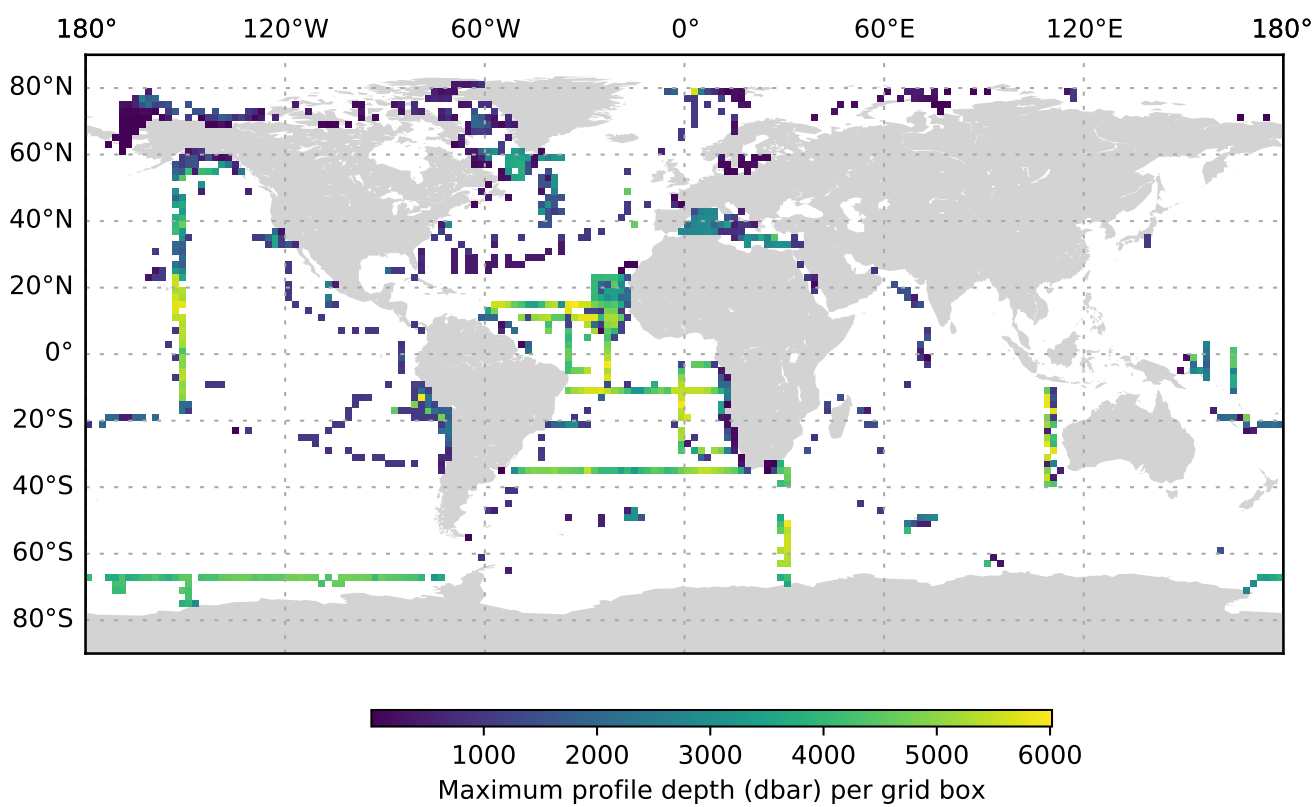


**Figure 4.** Maximum UVP5 profile depth per two degree grid box.

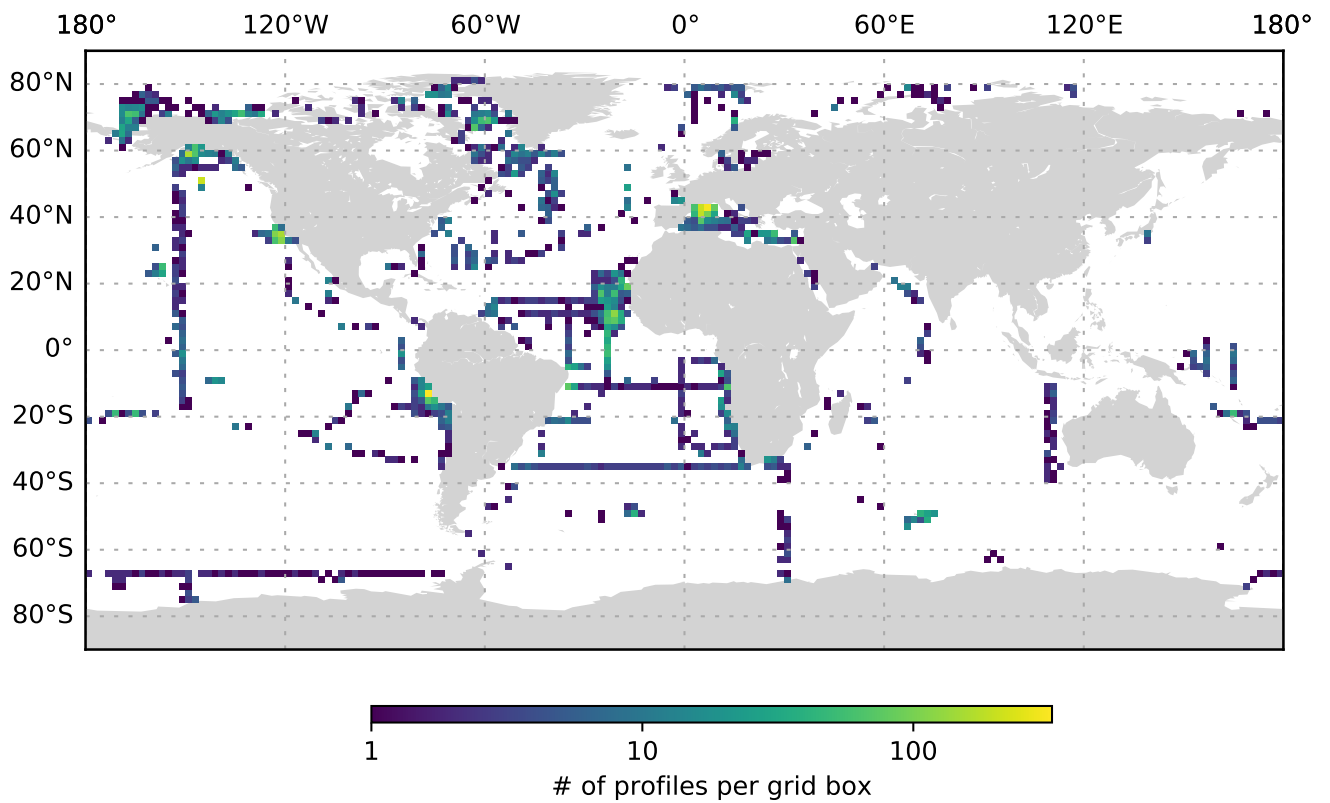
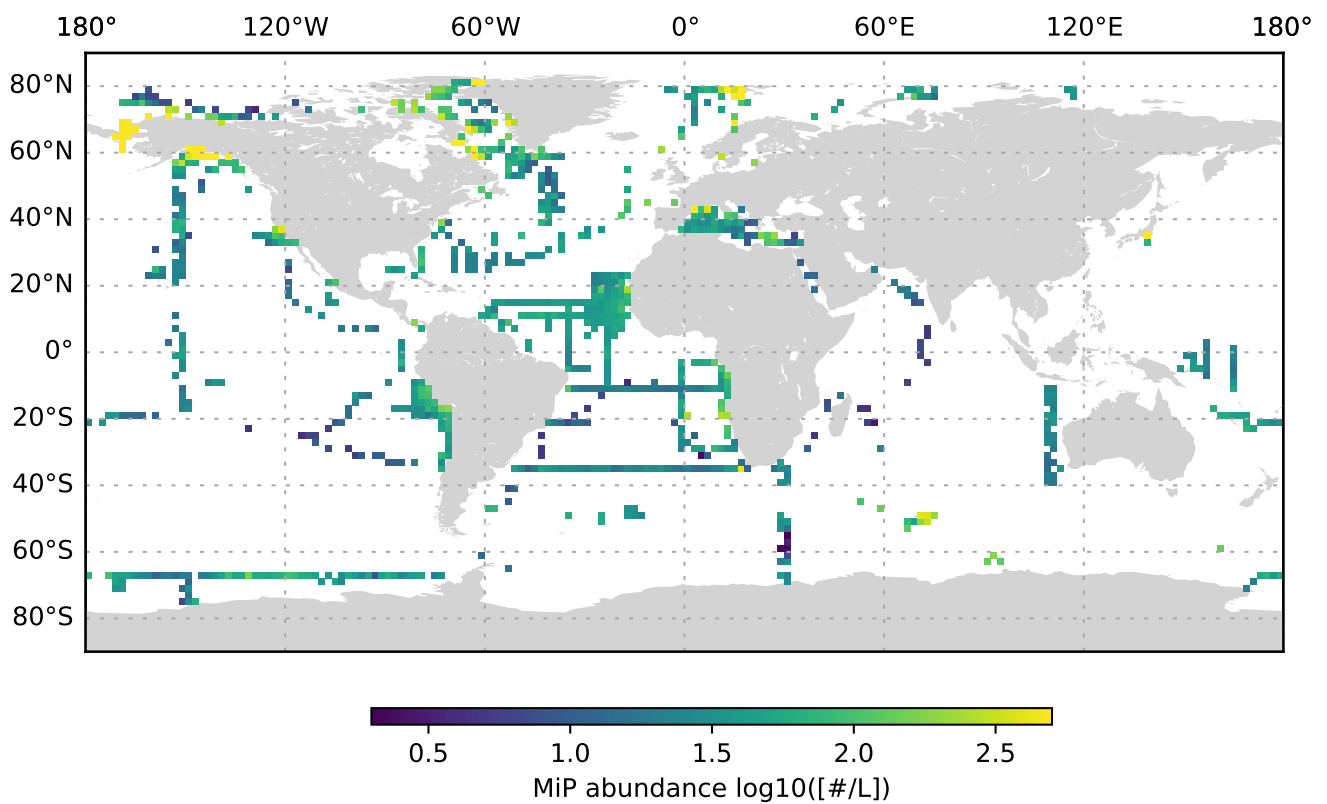


**Figure 5.** UVP5 data distribution per two degree grid box.



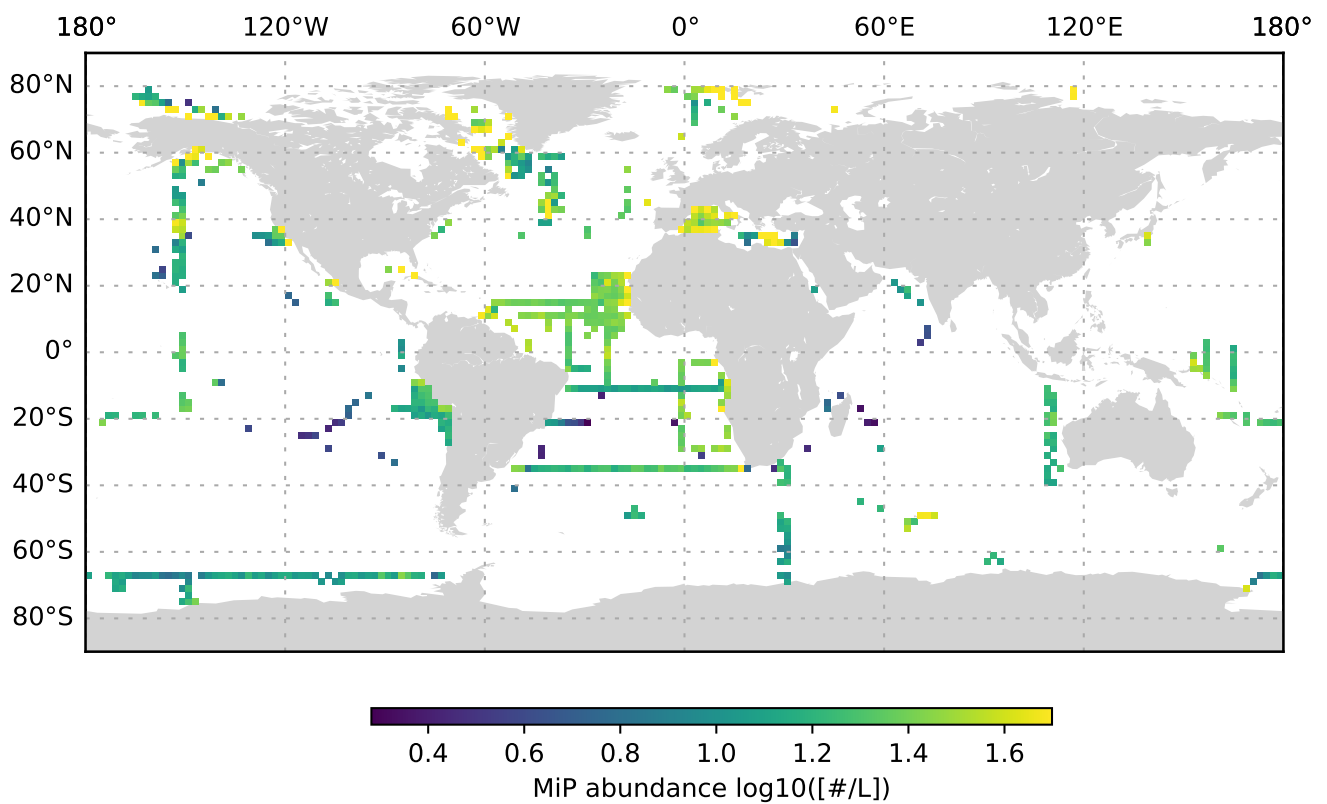
**Figure 6.**



MiP abundance (decadic logarithm) averaged for the 0 to 200 dbar depth layer and per 2 degree grid box. Only profiles at least 200 dbar deep were used for the analysis.



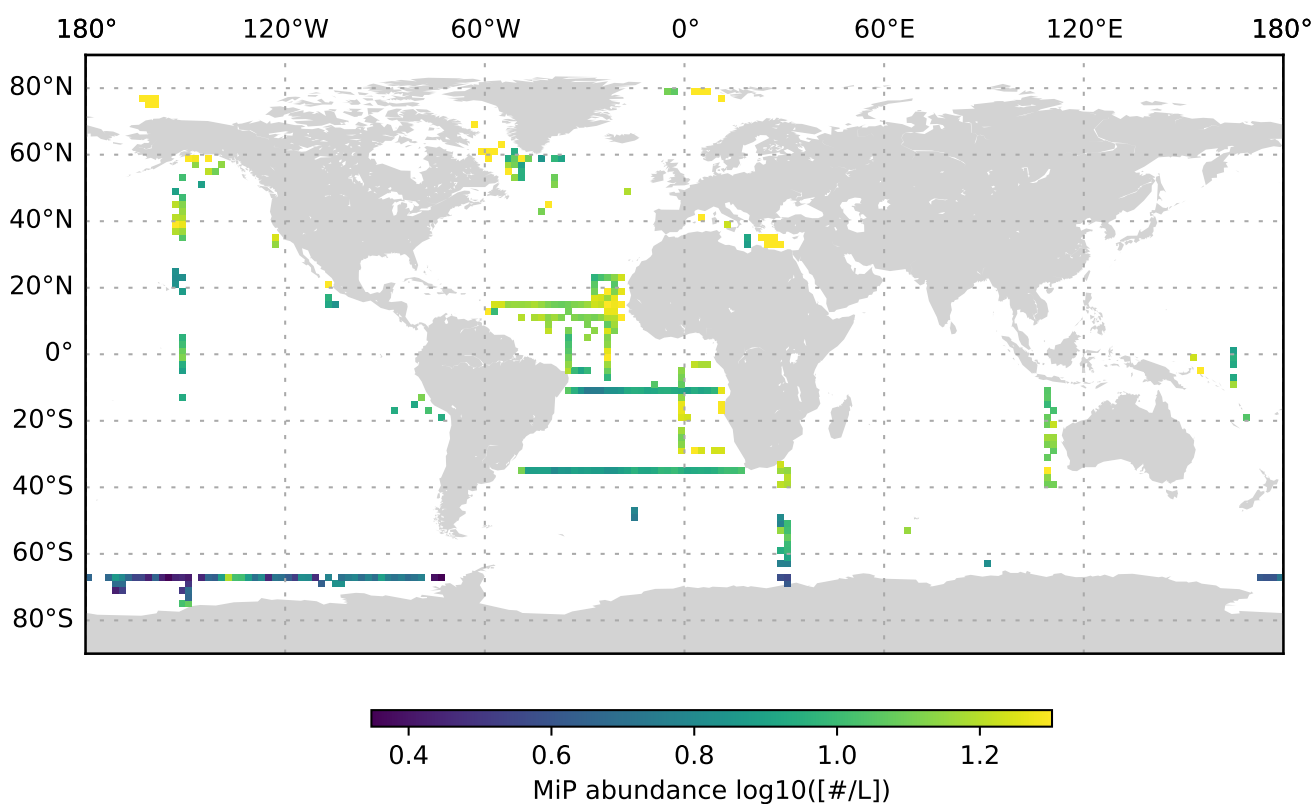
Figure 7.



MiP abundance (decadic logarithm) averaged for the 200 to 1000 dbar depth layer and per 2 degree grid box. Only profiles at least 1000 dbar deep were used for the analysis.



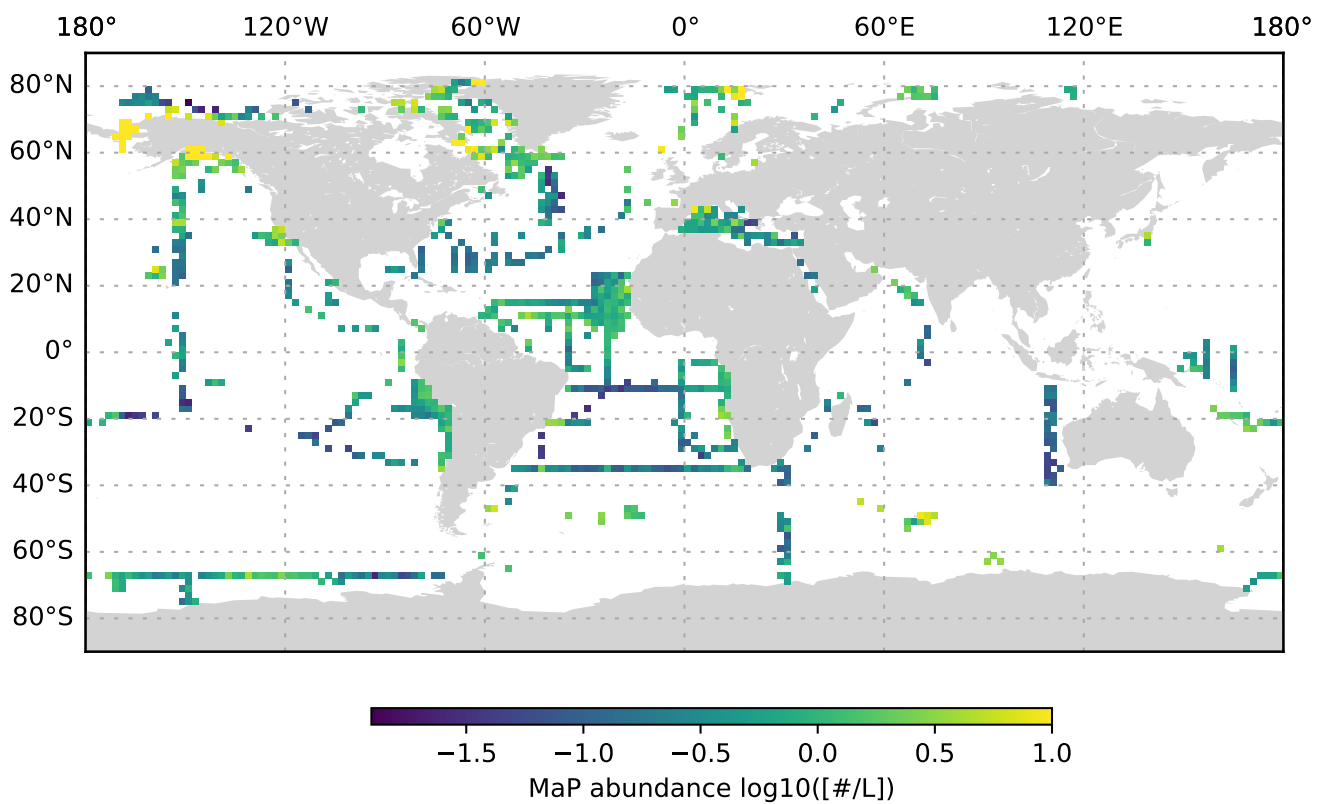
Figure 8.



MiP abundance (decadic logarithm) averaged for the 1000 to 3000 dbar depth layer and per 2 degree grid box. Only profiles at least 3000 dbar deep were used for the analysis.



**Figure 9.**

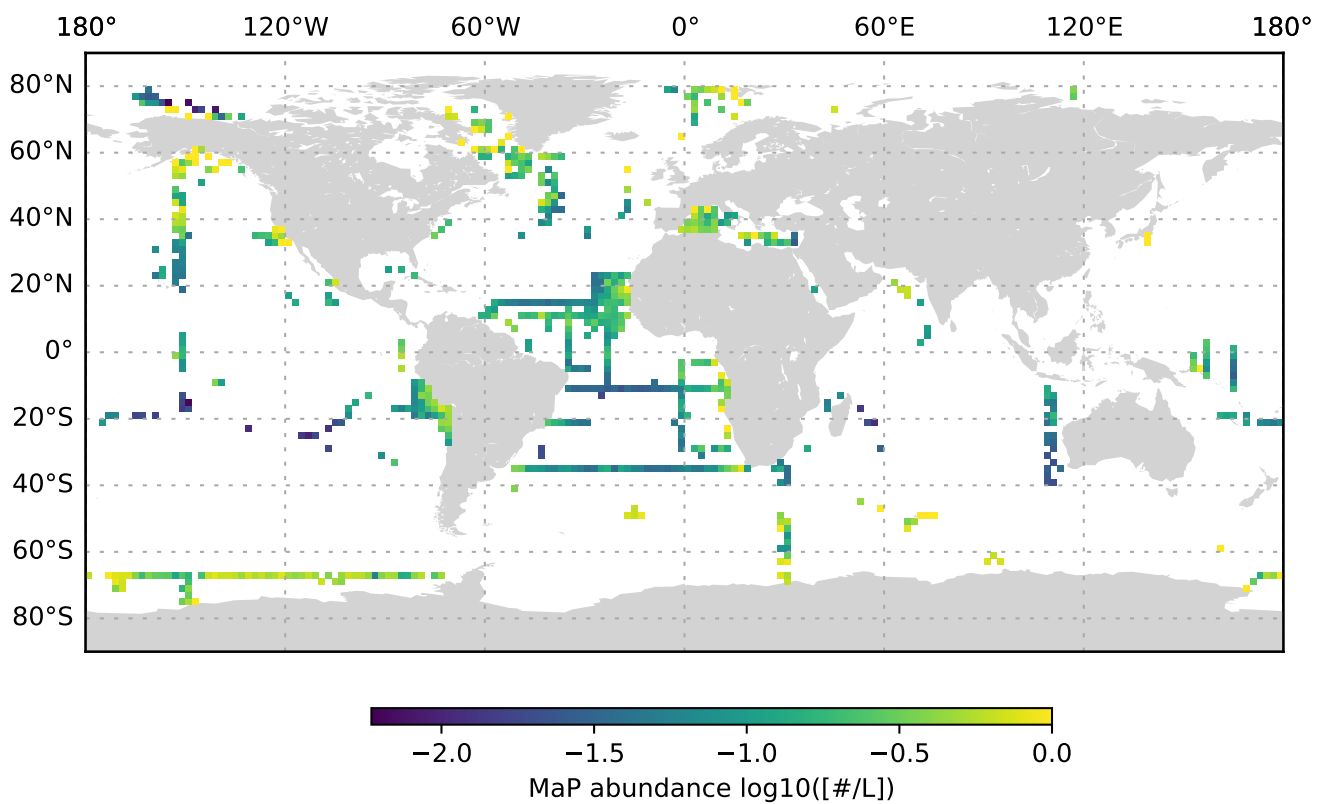


MaP abundance (decadic logarithm) averaged for the 0 to 200 dbar depth layer and per 2 degree grid box. Only profiles at least 200 dbar deep were used for the analysis.





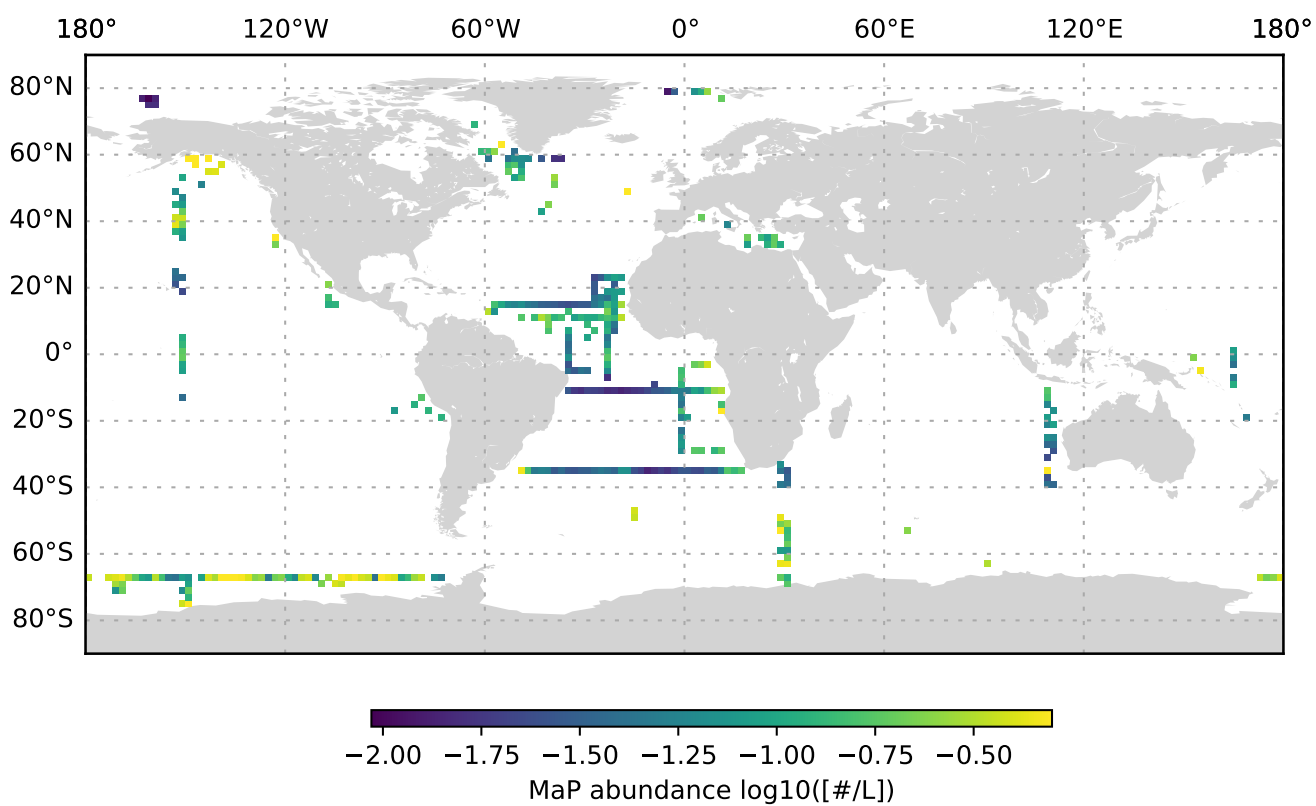
**Figure 10.**



MaP abundance (decadic logarithm) averaged for the 200 to 1000 dbar depth layer and per 2 degree grid box. Only profiles at least 1000 dbar deep were used for the analysis.



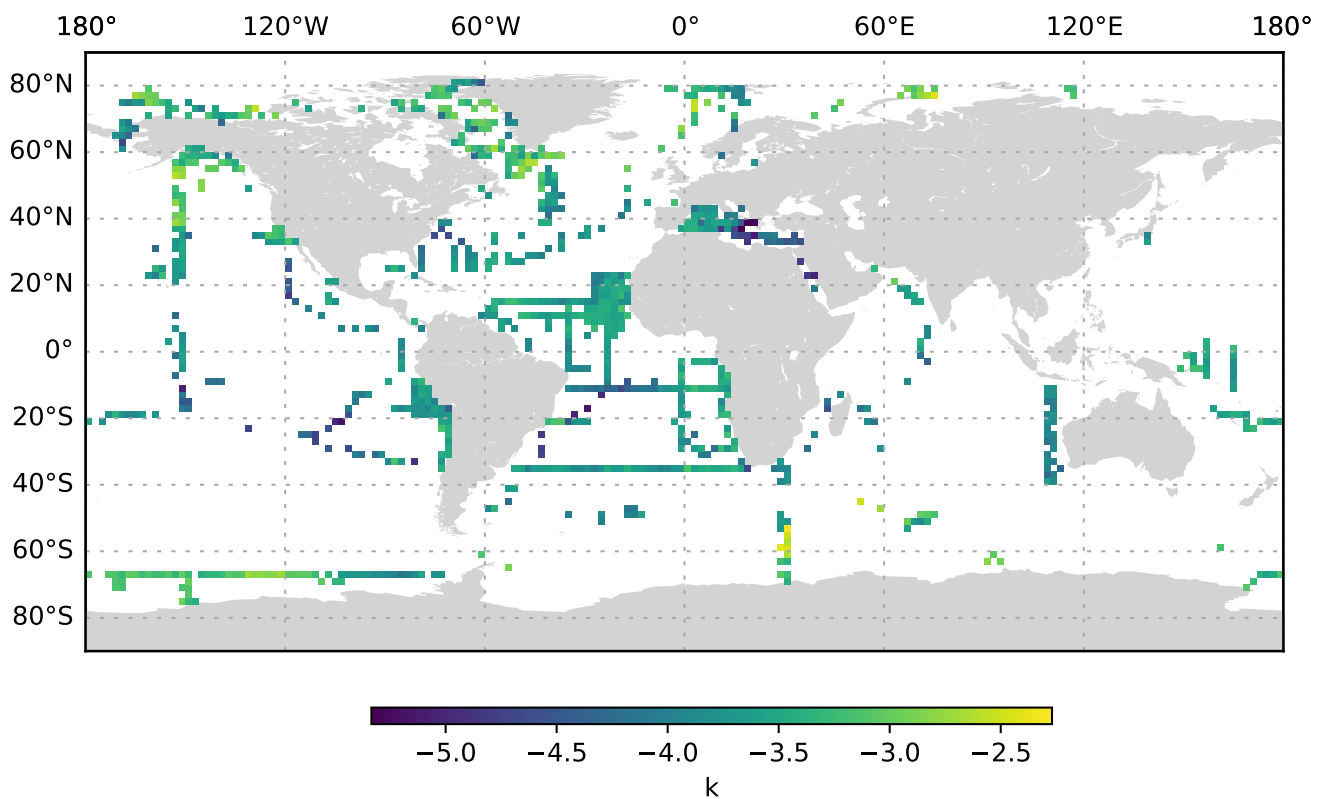
Figure 11.



MaP abundance (decadic logarithm) averaged for the 1000 to 3000 dbar depth layer and per 2 degree grid box. Only profiles at least 3000 dbar deep were used for the analysis.



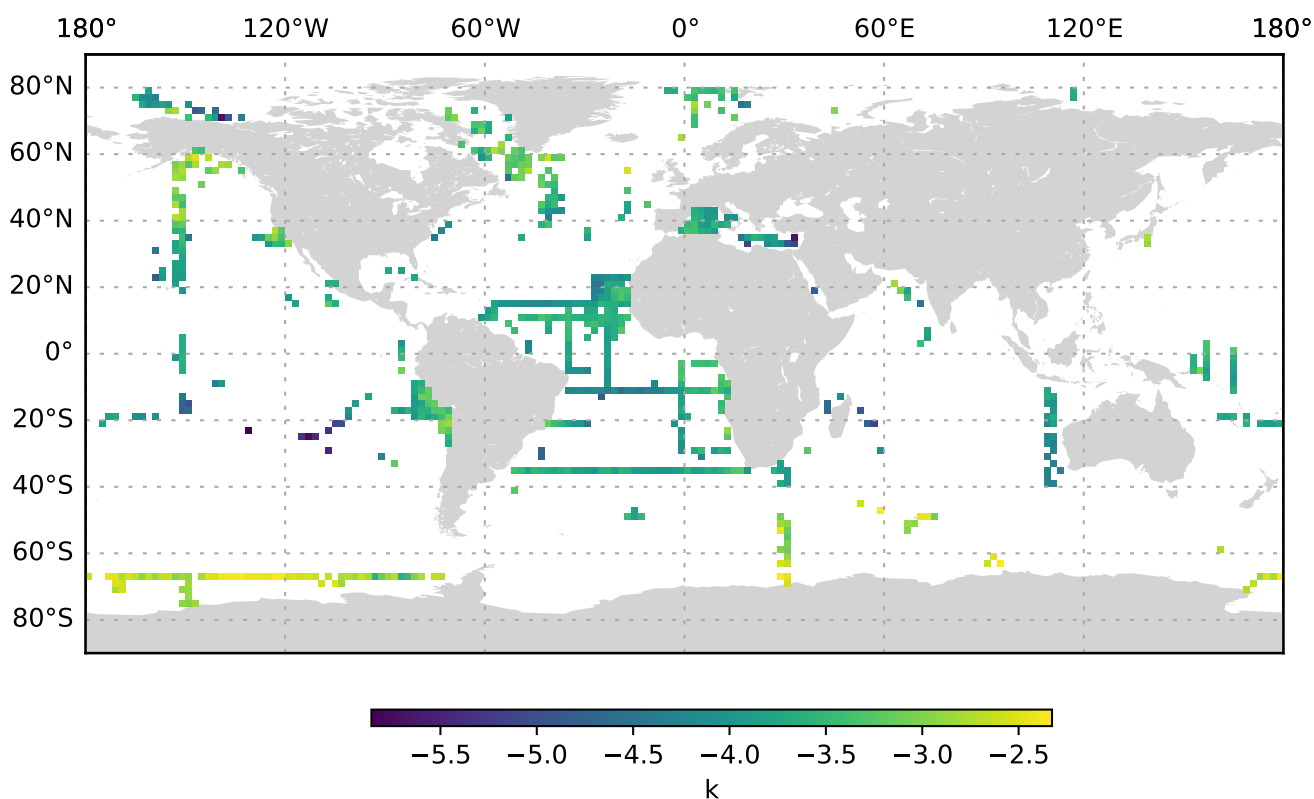
Figure 12.



k averaged for the 0 to 200 dbar depth layer and per 2 degree grid box. Only profiles at least 200 dbar deep were used for the analysis.



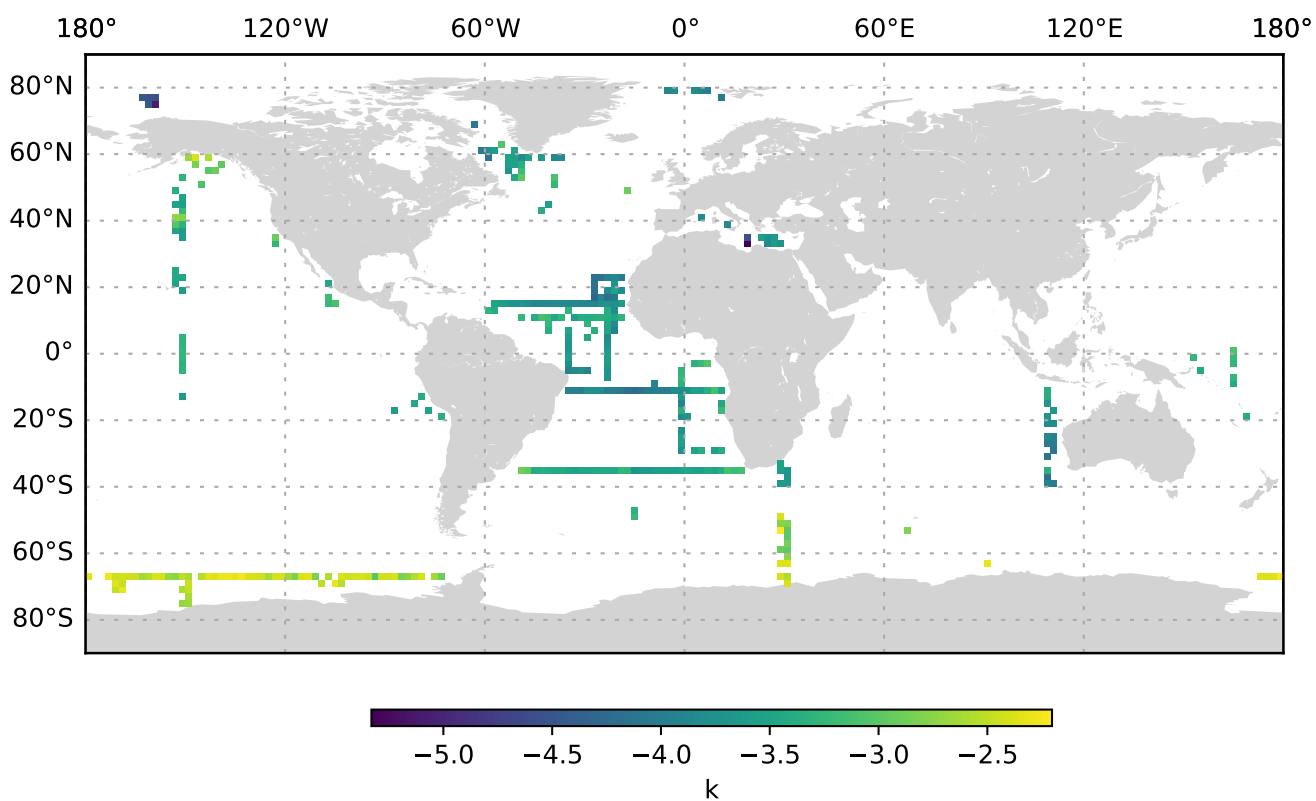
Figure 13.



k averaged for the 200 to 1000 dbar depth layer and per 2 degree grid box. Only profiles at least 1000 dbar deep were used for the analysis.



Figure 14.



$k$  averaged for the 1000 to 3000 dbar depth layer and per 2 degree grid box. Only profiles at least 3000 dbar deep were used for the analysis.